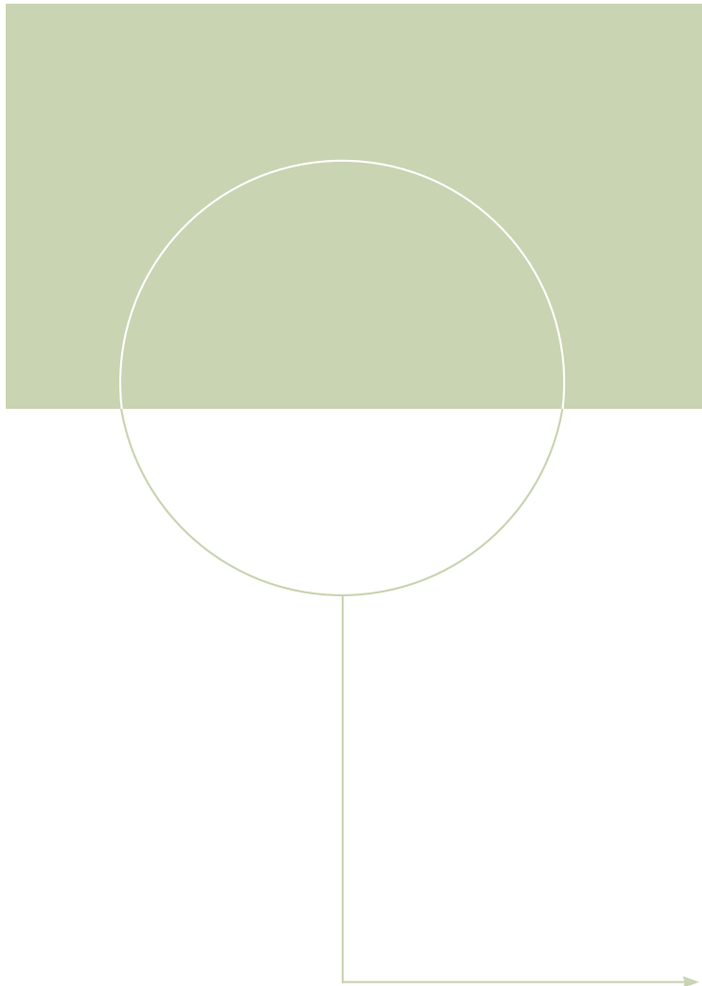

Master's thesis

2018

Oddbjørn Oseland

NTNU
Norwegian University of
Science and Technology
Faculty of Engineering
Department of Structural
Engineering

Oddbjørn Oseland

The effect of accelerated ASR on the mechanical properties and degree of damage of concrete over time - with and without uniaxial compressive stress

August 2018

NTNU
Norwegian University of
Science and Technology

NTNU
Norwegian University of
Science and Technology

NTNU

Norwegian University of
Science and Technology

The effect of accelerated ASR on the mechanical properties and degree of damage of concrete over time - with and without uniaxial compressive stress

Oddbjørn Oseland

Civil and Environmental Engineering
Submission date: August 2018
Supervisor: Terje Kanstad, KT
Co-supervisor: Klaartje De Weerdt, KT
Simen Sørgaard Kongshaug, KT

Norwegian University of Science and Technology
Department of Structural Engineering

Department of Structural Engineering
Faculty of Engineering
NTNU- Norwegian University of Science and Technology

ACCESSIBILITY:

OPEN

MASTER THESIS 2018

SUBJECT AREA: Concrete Technology	DATE: 31.08.2018	NO. OF PAGES: 61 + appendix

TITLE:

The effect of accelerated ASR on the mechanical properties and degree of damage of concrete over time – with and without uniaxial compressive stress

Virkningen på de mekaniske egenskapene og skadegraden av akselerert ASR over tid – med og uten en aksiell trykk spenning

BY:

Oddbjørn Wathne Oseland

SUMMARY:

The aim of this master thesis is to investigate the effect on mechanical properties and degree of damage in concrete exposed to accelerated Alkali-silica reaction (ASR) and uniaxial com-pressive stress, and test if the Stiffness Damage Test (SDT) still shows promising result as a tool to predict expansion when samples are restrained. It has previously been shown that uni-axial compressive stress inhibits expansion in the compressed direction. In addition, there has been shown a strong correlation between expansion, degree of damage and change in mechan-ical properties in concrete affected by ASR. A new experimental setup was designed to inves-tigate how external compressive stress affects the development of mechanical properties and degree of damage in concrete exposed to accelerated ASR.

18 prisms were cast and placed under different storage conditions with and without uniaxial compressive stress. Cylinders were drilled out parallel and perpendicular to the load direction at different times to study the effect of the restraints. The degree of damage and change in mechanical properties were investigated performing SDT followed by standard compressive strength tests on the cylinders. Elastic modulus, compressive strength and 3 different damage indices; Stiffness damage index (SDI), Plastic deformation index (PDI) and Non-linearity index (NLI), were calculated from the SDT.

The indices showed a strong logarithmic correlation with increasing level of expansion and the elastic modulus reduction showed a strong linear correlation with increasing expansion. The restrained prisms exposed to accelerated ASR showed lower level of expansion in restrained direction and similar expansion as the free prisms in unrestrained direction. Free ASR affected prisms showed a small reduction in compressive strength compared to the reference prism. However, when looking at the restrained prisms the result was small and vague.

All output parameters except compressive strength points to a lower degree of damage in the restrained prisms. The compressive strength showed weak correlation with expansion and seems to be a poor parameter to use when assessing ASR affected concrete. The damage indi-ces, SDI and PDI, showed promising result as tools to assess ASR damaged concrete struc-tures and potentially predict ASR expansion. The NLI showed weak correlation at low expan-sion level, render it less promising. For SDT to be a valid tool to predict expansion, different concrete recipes need to be tested and a thorough description of the test and calculation method needs to be defined.

RESPONSIBLE TEACHER: Terje Kanstad (NTNU)

SUPERVISOR(S): Terje Kanstad (NTNU), Simen Sørgaard Kongshaug (OsloMet), Klaartje De Weerdt (NTNU)

CARRIED OUT AT: Norwegian University of Science and Technology, NTNU

Preface

The experimental work described in this paper was carried out from January 2018 to August 2018. The work was executed to support Simen Sørgaard Kongshaug's PhD project (NTNU) entitled: "Numerical simulation of reinforced concrete structures affected by Alkali Aggregate Reaction (AAR)". The main task was to conduct and report the result from an experimental setup designed to investigate change in mechanical properties and degree of damage in concrete affected by AAR(ASR) under uniaxial compressive stress.

The experiments are funded by the Norwegian Public Roads Administration (Statens Vegvesen, SVV) through their research project "Better Bridge Maintenance", in which a research and development agreement have been signed between NTNU and SVV to perform research on the mechanical behavior of concrete affected by ASR. Simen Sørgaard Kongshaug (OsloMet – Oslo Metropolitan University) and Terje Kanstad (professor at NTNU) are responsible for the coordination of the research activities.

Acknowledgment

During the pre-project and working on my master thesis, I have had the opportunity to speak to many knowledgeable persons whom I would like to thank, as they took their time to speak with me and help me make better decisions. I would like to thank Simen Sørgaard Kongshaug (PhD-student at NTNU) as my copartner in designing the experimental setup and conducting the experiment, Terje Kanstad (professor at NTNU) for help during the design phase and making the necessary preparation, Max Hendrix (professor at NTNU and TU Delft) and Klaartje De Weerdt (associate professor at NTNU) for supervision during the project, PhD Jan Lindgård and Hans Stemland from SINTEF, Eva Rodum and Bård Pedersen From Statens vegvesen, for their insightful feedback and suggestions. I would also like to thank Knut Lervik, Erik Johansen and Roger Leistad from SINTEF concrete laboratory for their assistance during the experiment. A special thank need to be directed to my wife Sara for the immense support and help and to my family for support and being there when extra help was needed.

As this project changed from focusing on numerical modeling of ASR to design of a new test setup I have received supervision from both Terje Kanstad, Klaartje De Weerdt and Max Hendrix. My initial main supervisor during the pre-project was Max Hendrix, but as the focus of the project changed, he became less involved and I received supervision from Terje Kanstad and Klaartje De Weerdt. As Terje Kanstad was supervisor for Simen Sørgaard Kongshaug and hence more involved in the experiment, he became my main supervisor during my master thesis.

Summary

The aim of this master thesis is to investigate the effect on mechanical properties and degree of damage in concrete exposed to accelerated Alkali-silica reaction (ASR) and uniaxial compressive stress, and test if the Stiffness Damage Test (SDT) still shows promising result as a tool to predict expansion when samples are restrained. It has previously been shown that uniaxial compressive stress inhibits expansion in the compressed direction. In addition, there has been shown a strong correlation between expansion, degree of damage and change in mechanical properties in concrete affected by ASR. A new experimental setup was designed to investigate how external compressive stress affects the development of mechanical properties and degree of damage in concrete exposed to accelerated ASR.

18 prisms were cast and placed under different storage conditions with and without uniaxial compressive stress. Cylinders were drilled out parallel and perpendicular to the load direction at different times to study the effect of the restraints. The degree of damage and change in mechanical properties were investigated performing SDT followed by standard compressive strength tests on the cylinders. Elastic modulus, compressive strength and 3 different damage indices; Stiffness damage index (SDI), Plastic deformation index (PDI) and Non-linearity index (NLI), were calculated from the SDT.

The indices showed a strong logarithmic correlation with increasing level of expansion and the elastic modulus reduction showed a strong linear correlation with increasing expansion. The restrained prisms exposed to accelerated ASR showed lower level of expansion in restrained direction and similar expansion as the free prisms in unrestrained direction. Free ASR affected prisms showed a small reduction in compressive strength compared to the reference prism. However, when looking at the restrained prisms the result was small and vague.

All output parameters except compressive strength points to a lower degree of damage in the restrained prisms. The compressive strength showed weak correlation with expansion and seems to be a poor parameter to use when assessing ASR affected concrete. The damage indices, SDI and PDI, showed promising result as tools to assess ASR damaged concrete structures and potentially predict ASR expansion. The NLI showed weak correlation at low expansion level, render it less promising. For SDT to be a valid tool to predict expansion, different concrete recipes need to be tested and a thorough description of the test and calculation method needs to be defined.

Sammendrag

Målet med masteroppgaven er å undersøke effekten av akselerert Alkalireaksjon (ASR) og en aksielt trykk på de mekaniske egenskapene og skadegraden til betong. Det skal også testes om Stiffness Damage Test (SDT) gir lovende resultat som et verktøy til å estimere utvidelsen i prøver med fastholdninger. Det har allerede blitt vist at en aksielt trykk forhindrer utvidelse i last retningen. I tillegg har det blitt påvist en viss korrelasjon mellom utvidelse, skadegrad og forandring av mekaniske egenskaper i ASR påvirket betong. Et nytt eksperimentelt oppsett ble designet for å undersøke hvordan en aksiell trykk påvirket utviklingen av de mekaniske egenskapene og skadegraden til betong prøver eksponert for akselererte ASR.

De ble støpt 18 prismer som ble oppbevart under ulike forhold med og uten en konstant trykk last. Sylindere ble boret ut på ulike tidspunkt, med og på tvers av lastretning for å undersøke effekten av fastholdningene. Skadegraden og forandring i mekaniske egenskaper ble undersøkt ved å kjøre en Stivhet skade test (SDT) etterfulgt av en standart trykktest. Denne prosedyren gir fastheten, elastisitetsmodulen og 3 skadeindekser: Stivhet skade indeks (SDI), Plastisk deformasjons indeks (PDI) og ikke-linearitets indeks (NLI).

Skadeindeksene viste en sterk logaritmisk korrelasjon med økende utvidelse og reduksjon av elastisitetsmodul viste en sterk lineær korrelasjon med økende utvidelse. De fastholdte prismene eksponert for akselerert ASR hadde mindre utvidelse i den fastholdte retningen og liknende utvidelse på tvers av fastholdningen som de frie prismene. De frie prismene eksponert for akselerert ASR hadde en liten reduksjon i fasthet sammenlignet med referansene. Når vi undersøkte de fastholdte prismene var resultatene små og uklare.

Alle parametere peker på at det er mindre skade i de prismene som er fastholdt med unntak av fastheten. Fastheten viste en svak korrelasjon med økende utvidelse som tyder på at det er en dårlig parameter å bruke for å evaluere betong som er påvirket av ASR. Skadeindeksene, SDI og PDI, viste lovende resultat med tanke på å bruke SDT til å evaluere betong som er skadet på grunn av ASR og muligens også estimer utvidelsen. NLI viste svak korrelasjon ved lave utvidelser og anses derfor som mindre lovende. For at SDT skal bli er bra verktøy for å estimer utvidelsen må flere ulike betongresepter prøve i tillegg må det også lages en grundig beskrivelse av test metoden og hvordan indeksene regnes ut.

Table of content

List of figures

List of tables

1 Introduction

Concrete is the most used building material in the world. There are several reasons for this, amongst others flexibility, price and durability. One drawback of using concrete is the high environmental footprint that it leaves. A way of lowering the environmental footprint is to increase the service life of existing concrete structures. To achieve this, a good understanding of how the properties of concrete develop with age, and how different deterioration mechanisms evolve over time are necessary.

As a composite material consisting of cement, aggregate, water and additives, there are countless of factors that influence the development of concrete. When mixing water and cement minerals, chemical reactions causes concrete to harden, a process called hydration. The hydration process is a complex reaction influenced by temperature, access of water, cement and additives. There have been many studies on hydration of Portland cement, which is the most common cement type, and the process is well known and described in detail by e.g. Gartner et al. [1]. To increase performance, e.g. in terms of strength, sulfate resistance and permeability, and to lower the environmental footprint, concrete producers replace some of the cement with different byproducts from the industry like silica fume, fly ash or blast furnace slag. All cement replacements highly affects the hydration process and hence the development of concrete.

Over time concrete starts to deteriorate due to forces of nature, which can lead to different damage mechanisms depending on the exposure and quality of concrete. Reinforcement corrosion, freeze-thaw, fatigue and alkali-aggregate reaction (AAR) are some of the possible deterioration mechanisms acting on concrete structures. This study focuses on ordinary Portland cement, without replacement of cement, and on a subgroup of AAR, called alkali-silica reaction (ASR), as it is the most common amongst the AAR subgroups. In this reaction, siliceous aggregates react with alkaline pore solution in the concrete.

ASR has been a known deterioration problem worldwide since about 1940, while it has only been a recognized problem in Norway since the 1980-1990 [2]. Many of the common aggregates around Norway are so called alkali reactive, which means that the aggregates are prone to develop ASR under certain conditions. This combined with the harsh weather especially along the coast makes ASR a viable and important deterioration mechanism in Norway, which we should be aware of and try to understand. It is already a known problem in older bridges e.g. Elgeseter Bridge in Trondheim [3].

That ASR provides problems that need attention, is made clear in one of the projects run by The Norwegian Public Roads Administration (Statens vegvesen, SVV) from 2017 to 2021 called "Better Bridge Maintenance (Bedre Bruvedlikehold)", where subproject 3 covers ASR and states: "This project focuses on the load-bearing capacity and service life of bridges and ferry quays with damages related to alkali silica reactions. This project will also focus on corrective and preventive maintenance measures increasing the service life of bridge structures with alkali silica reactions" [4].

1.1 Basic mechanisms of Alkali-silica reaction

For ASR to occur in concrete, three requirements must be met: 1: The aggregates need to be reactive, 2: the concrete needs to have a high concentration of alkali metals and 3: water needs to be present (high moisture level). This can be illustrated by the triangle showed in figure 1. If one of the criteria is not met, the reaction stops.

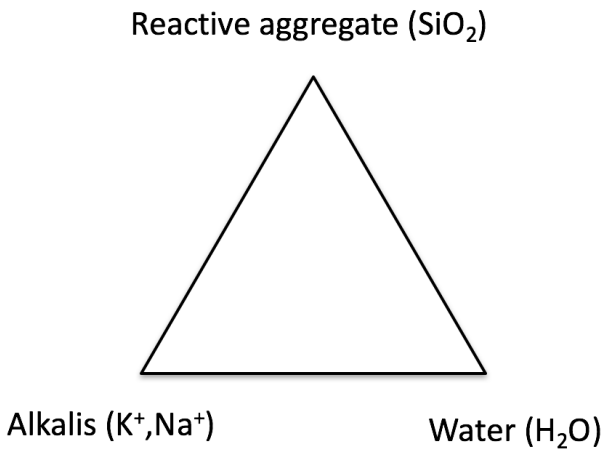

Figure 1 Requirements triangle for ASR [4].

ASR is as mentioned a chemical reaction between the aggregate and the alkaline pore solution in concrete. The alkaline pore solution is formed by presence of alkali metals consisting of sodium (Na^+) ions and potassium (K^+) ions. The main source of alkali metals is the cement fraction of concrete, though aggregates or other additives could potentially contribute. For the reaction to start, the aggregate must contain soluble silicon oxide. When soluble silicon oxide is present it is likely to be dissolved if the pH in the concrete pore solution is high e.g. 13.5 [2]. High content of alkali metals present together with calcium hydroxide can produce a pH higher than 13.5. The reaction product between dissolved silicon oxide and alkali metals is a viscous alkali silica gel [5].

Water plays two roles in ASR: First, it is necessary to dissolve the silicon oxide, and secondly, water is absorbed by the viscous alkali silica gel. The latter causes swelling of the gel resulting in an increase in volume. The increased volume creates a pressure at the reactive sites and tensile stresses in the surrounding material, which eventually results in micro cracking, expansion (strain), loss of strength and changes in other mechanical properties as showed by Lindgård et al. [2].

1.2 Modeling ASR to increase service life

ASR is a complex reaction and at present time, there is no consensus in the research literature on how to predict and calculate the effect of ASR in terms of expansion and performance of the concrete. As Karthik et al. [6] states, several numerical models have been suggested to predict the expansion from ASR to a varying degree of success, but the most accurate models are complex.

Even though there exist a handful of material models used to describe ASR, many of them rely on parameters calculated from laboratory samples that are free to expand in all directions. This is not the case in most concrete structures. In many concrete structures, there are several levels of restraint, from steel reinforcement bars to connections between structural members, concrete and ground.

1.3 Effects of restraints on ASR affected concrete

Berra et al. [7] investigated how different level of uniaxial compressive stresses, ranging from 0.17 – 3.5 N/mm^2, affected the degree of expansion in each direction. Their study showed larger expansion reduction with increasing level of restraint and increasing expansion in unrestrained direction with increasing level of restraint compared to samples free to expand in all directions. Gautam et al. [8] investigated multiaxial restraints, with compressive stresses varying between 0, 3.9 and 9.6 MPa, and how it affected the degree of expansion in concrete affected by accelerated ASR. Their study showed similar results as Berra et al. [7] with large decrease of expansion in restrained direction and increasing expansion in unrestrained directions compared to free samples. Both Gautam et al. [8] and Berra et al. [7] showed that restraints affect the degree of expansion in concrete affected by accelerated ASR. Neither of the mentioned studies investigated how the change in expansion level affected the properties of concrete and if the reported transfer of expansion is universal for all types of concrete affected by ASR restrained in one direction.

The effect of restrain on ASR affected concrete have also been investigated by Jones and Clark. [9] They investigated cylinders exposed to 1,2, 4 and 7 MPa constant compressive stress. Their result showed that a stress level of about 3MPa reduced the expansion to about 20% relative to samples with free expansion. They reported no significant change perpendicular to the load direction, contrary to Gautam et al. [8] and Berra et al. [7]. Jones and Clark. [10] investigated the effect different level of restraints had on the mechanical properties of ASR affected concrete. They reported increasing reduction in both compressive strength and elastic modulus with increasing expansion. The relation seemed to follow a decreasing concave up curve.

1.4 Accelerated conditions

Like the previously mentioned studies of Berra et al. [7], Gautam et al. [8] and Jones and Clark. [9,10], this study also uses accelerated ASR conditions speed up the reaction in concrete samples. In normal exposure conditions, ASR is a slow reaction and it could take several decades before the ASR becomes visible. High temperature and high humidity are normally used to accelerate the reaction in laboratory testing. This makes the correlation between laboratory and field conditions complicated. One part of this disparity between laboratory and field testing is due to leaching, which according to Rivard et al. [11] is a result of condensation on the concrete surface which is moved by gravitation to the bottom of the storing container. This results in a loss of alkali metals at the surface which causes a diffusion force that is transferring alkali metals from the prisms core to the outer surface. Rivard et al. [12] showed that real life concrete structures are not suffering from considerable leaching as opposed to laboratory samples. This is likely due to a high volume to surface ratio in field concrete structures compared to laboratory samples. When leaching occur in laboratory testing, there is a problem with a possible loss of expansion as Lindgård et al. [13] showed. In turn, this could affect the degradation of mechanical properties.

Another important aspect to consider when exposing the samples to accelerated condition, high temperature and humidity, is hydration. The high temperature affects the development of mechanical properties in concrete. Balendran et al. [14] investigated the effect of different curing temperature during the first 7 days and equal conditions after 7 days had on the mechanical properties of concrete samples. They reported a reduction in compressive strength at the 28 days test. The same reduction in compressive strength with increasing temperature was found when Tan and Gjorv. [15] investigated the performance of concrete cured at different temperatures and humidity. They also reported higher strength in cubes first stored 3 and 7

days in water followed by storage in air, with 50% relative humidity(RH), compared to samples stored 28 days in water. It is not clear if their cubes had the same temperature and moisture content during the compressive strength test. This could affect the result. Shoukry et al. [16] investigated the effect different moisture contents and temperatures had on mechanical properties when curing conditions were identical until right before testing. They reported reduction in compressive strength with increasing temperature and moisture content at time of testing. Brooks et al.[17] studied the effect of dry and wet storage over a time period of 30 years, and they found larger compressive strength in dry stored samples than wet stored samples. High temperature and humidity clearly interfere with the measured change in mechanical properties.

1.5 Compressive strength

The loss in compressive strength due to ASR is according to Sanchez et al. [18] much lower than the loss in elastic modulus and tensile strength. They point to an expansion of 0.1% as the point when the loss of compressive strength needs attention. When the expansion goes beyond 0.3%, the loss can be critical and strong attention may be needed. Barbosa et al. [19] investigated ASR in a field study of a damaged bridges. They compared the mechanical properties of cores drilled parallel and perpendicular to the visible crack pattern. Their study showed a significant reduction in the compressive strength perpendicular to the visible crack pattern. Since their test cylinders were taken from a bridge in-situ, expansion measurement was not presented, and the undamaged compressive strength was estimated. However, a reduction in compressive strength and a more ductile behavior were apparent.

Marzouk et al. [20] investigated the change in mechanical properties of concrete exposed to two different accelerated ASR conditions for 12 weeks. In one condition, the samples were stored in water keeping 80°C, and in the other the samples were stored in 80°C NaOH solution. As opposed to Sanchez et al. [18] and Barbosa et al. [19], Marzouk found no reduction in compressive strength after curing in water using highly reactive aggregates. On the contrary, an increase in compressive strength compared to the 28 days compressive strength was reported. The increase was explained by increasing hydration due to the high storage temperature. This statement contradicts the work done by Balendran et al. [14] showing lower compressive strength in sample stored in high temperature not suffering from ASR. However, Marzouk reported a significant reduction, of 24%, in compressive strength in similar samples stored in NaOH solution. This difference reported by Marzouk is likely due to an effect of leaching and lack of alkali metals, resulting in less ASR development in the samples stored in

water. Nevertheless, the seemingly lower ASR development in the sample stored in water, suggest that the compressive strength increase due to hydration is larger than the reduction due to ASR.

1.6 Elastic modulus

Marzouk et al. [20] reported a reduction in elastic modulus on samples that displayed increased compressive strength and a large, 81%, reduction in elastic modulus for samples stored in NaOH solution. Giaccio et al. [21] have in conformity with Marzouk showed that the elastic modulus is strongly affected by ASR, while the effect on compressive strength is only limited or nonexistent. The sample with the largest expansion did not display the lowest elastic modulus and compressive strength. However, the ASR affected concrete with high expansion did display a much lower elastic modulus compared to the concrete samples with small degree of expansion. This corresponds well with Sanchez et al. [18]. They showed that the reduction is dependent on both the aggregate and degree of expansion. In addition to the large reduction in compressive strength perpendicular to cracks reported by Barbosa et al. [19], the results also showed large reduction of elastic modulus perpendicular to crack pattern compared to elastic modulus parallel to cracks. Therefore, it can be concluded that change in elastic modulus due to ASR is a result of the aggregate used, the level of expansion, the access of alkali metals and occurring cracks.

Elastic modulus is highly affected by the concrete mix and the initial elastic modulus is not necessarily known when a concrete sample is taken from a concrete structure. The initial elastic modulus can be estimated by using cyclic loading, looking at the unloading of the last load cycle. The initial elastic modulus is then given as the slope of a line drawn from the top of the last load cycle to a point 2.5MPa lower on the unloading curve as described by Stemland and Haugen [22]. This differ from the standards by looking at the unloading of the last load cycle instead of loading of the first cycle as described in NS-EN 12390-13 [23]. The reason for using the method described by Stemland and Haugan [22] is that it can be performed after running the Stiffness damage test.

1.7 Stiffness Damage Test (SDT)

The stiffness damage test (SDT) dates back to the mid 1980 when it was presented by Crisp et al. [24] as a way of quantifying the degree of damage in concrete due to ASR. They performed 5 load cycles from 0 MPa to 5.5 MPa in compression with a load/unload speed of 0.1

MPa/s. The SDT was performed on over 1000 concrete samples, where they looked at three different diagnostic parameters:

- Elastic modulus: Given as the average secant elastic modulus from the last four load cycles. Damaged concrete has a lower secant elastic modulus.
- Hysteresis area: The average hysteresis loops during the last four load cycles. Damaged concrete tends to have a greater energy loss then undamaged concrete. Hence a bigger hysteresis area.
- Plastic deformation: The total plastic deformation accumulated over the five load cycles. Damaged concrete show a bigger accumulated plastic deformation and larger total deformation during testing.

When evaluating the SDT Sanchez et al. [18] used different maximum load levels. Lower load levels showed less concluding result. A recommended load level of 40% of the 28 days design compressive strength was proposed, as the output parameters were clearer, and the test was still non-destructive for both aggregates investigated in their study. This is the same level as recommended by ASTM [25] in standard testing of elastic modulus.

In Sanchez et al. [26] work on establishing a practical approach to use the SDT, they concluded that the output parameters, hysteresis area and the plastic deformation could be misleading and suggested two indices as the main output parameter, as illustrated in figure 2. The indices are:

- Stiffness Damage Index (SDI): The sum of the hysteresis area (SI) divided by sum of total energy (SI + SII) for each load cycle. Illustration of SI and SII is shown in figure 2.
- Plastic Deformation Index (PDI): The plastic deformation accumulated during the SDT (DI) divided by the total deformation measured at max load in the last cycle (DI + DII). Illustration of DI and DII is shown in figure 2.

Sanchez suggested a third index to calculate along SDI and PDI, showing promising result when trying to estimate degree of damage and the alignment of cracks. This third index was elaborated and tested along with SDI and PDI in Sanchez et al. [27] work using SDT on 20 different concrete mixes. It was found to be an interesting complementary index to calculate. The index is:

- Non-linearity index (NLI): The slope of a straight line drawn from origin to half of the maximum load divided by the slope of a straight line drawn from origin to maximum load in the first load cycle. The lines are drawn in figure 2.

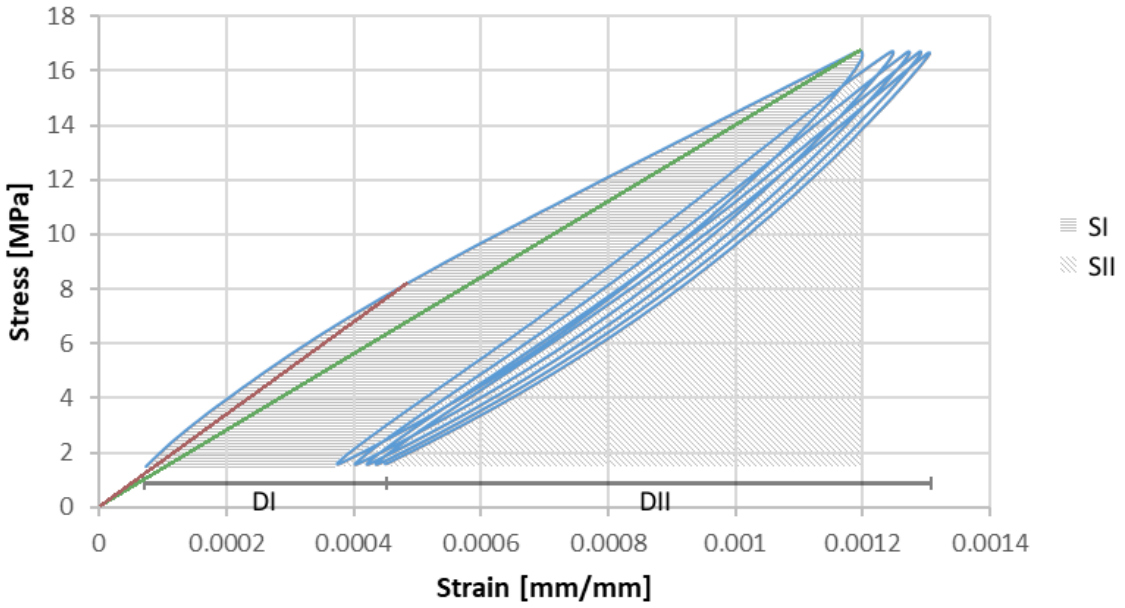

Figure 2. Illustrating the indices calculated from the stiffness damage test.

Sanchez et al. [26] declare SDT as a potentially powerful tool of assessing the degree of damage in concrete structure affected by ASR, and other damaging mechanisms acting on concrete. This was further supported by Giannini et al. [28] as SDI and PDI showed promising result when used to characterize concrete affected with delayed ettringite formation. For SDT to reach its full potential, further testing on different aggregates, other conditions, etc. is needed.

2 Objective

The main objective of this study is to investigate how ASR and uniaxial compressive stress affect the elastic modulus, compressive strength and the degree of damage in a selected concrete recipe, and how the deterioration evolves over time under accelerated conditions and how it is related to the increasing expansion.

Furthermore, the stress-induced anisotropy in the concrete due to the uniaxial compressive stress is of great interest. This will be characterized by the degradation of the mechanical properties, and the damage indices from the stiffness damage test (SDT). In addition, some cylinders will be split, and their plane sections will be impregnated with fluorescent epoxy and investigated under UV- light. Due to limitations of the scope of a master thesis, the latter is not included in this report.

The report contains a summary of the literature study, a description of the experimental setup, the results from the stiffness damage test and the development of the mechanical properties, a discussion about the experimental setup, the results, a discussion of the meaning of these results along with some concluding remarks.

2.1 Research questions

Can the stiffness damage test (SDT) be used as a tool to estimate the ASR expansion and predict the corresponding changes in mechanical properties? To what extent will the uniaxial load condition influence the performance of the SDT?

2.2 Approach

In order to fulfill the objective and answer the research question, a set-up that keeps a constant stress in one direction was designed and constructed. A large number of prisms was cast, some of them were loaded by a uniaxial compression, while the rest was unrestrained. From each prism, four cylinders were drilled out: Two parallel and two perpendicular to the loading direction. The stiffness damage test as described by Sanchez et al.[18], with subsequent loading until failure, were conducted on all cylinders. This was the basis for measuring the compressive strength and elastic modulus and calculating the damage indices denoted SDI, PDI and NLI. During the stiffness damage test there is a possible plastic deformation occurring, which might influence the measured compressive strength. To get additional information about the compressive strength development, three cubes exposed to accelerated condition and three cubes exposed to reference condition were tested at the same time as the drilled cores were tested. All samples were cast with the same concrete mix to make the evaluation of

the results simpler as the elastic modulus and compressive strength were initially the same for all samples.

3 Materials and method

3.1 Materials

The cement used in this test is a Portland industry CEM I 42.5R cement according to (EN 197-1) with high alkali content (1.24% Na_2O_{eq}) and Blaine specific surface of 575 m^2/kg. This cement has a surplus of alkali. By choosing this specific cement the impact of leaching on expansion is limited.

The aggregate consists coarse aggregate from Ottersbo and fine aggregate from Årdal with a ratio of about 60:40 (coarse:fine). The fine aggregate is non-reactive natural sand 0-4 mm with the major parts being granites and gneisses. The coarse aggregate is reactive crushed cataclasite 4-16 mm [2]. These same aggregates are used in previous ASR experiments both at SINTEF and Norcem [2].

The concrete mix was selected after consulting Jan Lingård (SINTEF), Eva Rodum (SVV) and Bård Pedersen (SVV), on the basis that the recipe is well documented with regard to ASR testing and will surely expand more than 0.3% during the testing period. The mix recipe used in this experiment is identical to the one used by an ongoing ASR field experiment run by SVV described in SVV report number 465 [29]. The concrete mix recipe is shown in table 1.

Table 1. Concrete mix recipe [23].

Concrete mix		Density [kg/m^3]	Batch 1 [kg]	Batch 2 [kg]	Totalt [kg]
Portland industry CEM I 42,5R		457	68,55	68,55	137,1
Årdal sand 0-4 mm	Dry weigth	667	100,05	100,05	200,1
Ottersbo 4-8 mm	Dry weigth	172	25,8	25,8	51,6
Ottersbo 8-11 mm	Dry weigth	518	77,7	77,7	155,4
Ottersbo 11-16 mm	Dry weigth	345	51,75	51,75	103,5
Sika FB-2		1,4	0,21	0,21	0,42
Water		217	32,55	32,55	65,1
Alkali-content, Na2O-equ.		5,6			
w/c-ratio		0,475			

The mix recipe contains 457 kg/m^3 cement with a water-to-cement ratio (w/c) of 0.475. This will result in an alkali content of 5.6 kg/m^3. The mix for the sample exposed to accelerated conditions is identical to the mix used in the reference samples. Instead of using different

mixes to get ASR in some sample and no ASR in reference sample, which would affect both the mechanical properties and how it is affected by ASR, different storing conditions are used.

To attain control over the moisture in the aggregates, water is added until excessive water appears. Then the moisture is measured by taking out a small part of the aggregate and weighing the sample, then oven drying the sample until all water is evaporated before weighing the sample again. The percent of water in the aggregate is calculated as shown in formula (1):

$$percent\ of\ water = \frac{m_{wet} - m_{dry}}{m_{dry}} \times 100 \quad (1)$$

m_{wet}: weight of the wetted aggregate [kg]

m_{dry}: weight of the oven dried aggregate [kg]

After the aggregates were wetted and the percent of water were calculated, the aggregates were placed in watertight plastic containers until mixing of the concrete. This was done to hinder the aggregates from drying. The weighed-in cement, aggregates, water and additives along with measured slump, air content and density are presented in Appendix A.

In total 20 prisms (230 x 230 x 230 mm) and 27 cubes (100 x 100 x 100 mm) were cast. To cast all samples 300 liters of concrete were necessary, which were cast in two batches of 150 liters each. The form was filled and compressed manually as described in NS-EN 12930-2. After smoothing the top, the filled forms were stored at 20°C for 24 hours under plastic cover. They were then demolded, put under a soaked linen bag, wrapped in plastic and stored at 20°C for 8 days.

After the initial hardening 10 prisms and 12 cubes were stored in conditions similar to the description in RILEM AAR-4.1 [30], which was 60°C and 100% RH. On the first day of exposure, five prisms were fastened to a stress of roughly 0.3 MPa. The next day, the bolts were fastened to reach the desired stress of 3 MPa. Hereby, these prisms are referred to as restrained prisms and the direction of the applied stress is called restrained direction and z-direction. This two-step procedure was done to minimize the interference with thermal expansion during the heating of the system and prisms, from 20°C to 60°C. The 4 unrestrained reference prisms (not exposed to accelerated conditions) and 15 cubes were left under the soaked

linen bags packed in a plastic sheet. Another 4 prisms were placed under constant compressive stress of 3MPa in a room that was keeping 20°C and 50% RH, hereby called restrained reference prisms. This was different humidity condition than the unrestrained reference prisms were exposed to. The reason for this was that an existing machine was used, which is primarily used to measure creep. The machine was already standing in a room with the given conditions and unfortunately, changing the settings in the room was not an option. All reference prisms are stored at room temperature (20°C) enclosed with wet linen bags and plastic sheets, which made the relative humidity close to 100%. This resulted in 10 prisms and 12 cubes stored at 60°C, where 5 prisms were restrained (RP60) and 5 prisms along with 12 cubes were free to expand in all direction (FP60 and FC60). 8 prisms and 15 cubes stored at 20°C, where 4 prisms were restrained (RP20) and 4 prisms along with the 15 cubes were free to expand in all direction (FP20 and FC20). The casted prisms and cubes and the associated conditions are presented in table 2.

Table 2. Show the number of samples in the different storing conditions.

Condition	Amount	Type	Temperature[°C]	Humidity	Restrained/Free
RP60	5	Prism	60	~100%	Restrained
FP60	5	Prism	60	~100%	Free
RP20	4	Prism	20	~50%	Restrained
FP20	4	Prism	20	95-100%	Free
FC20	15	Cube	20	95-100%	Free
FC60	12	Cube	60	~100%	Free

3.2 Set-up

An equipment highly inspired by Berra et al. [7] and Kagimoto et al. [7,31] was designed to keep control of and measure the load applied to the restrained prisms, as shown in figure 3. The setup consists of two outer plates connected by four threaded steel bars kept tightly together by bolts. To sustain constant stresses, a loading cell is placed between the outer plate and a plate connected to the prisms. The loading cell is connected to a computer that displays and logs the load continuously. A layer of teflon was added between the prisms and the steel plates to minimize the degree of friction between the steel plate and the concrete as the concrete expand when ASR starts to develop.

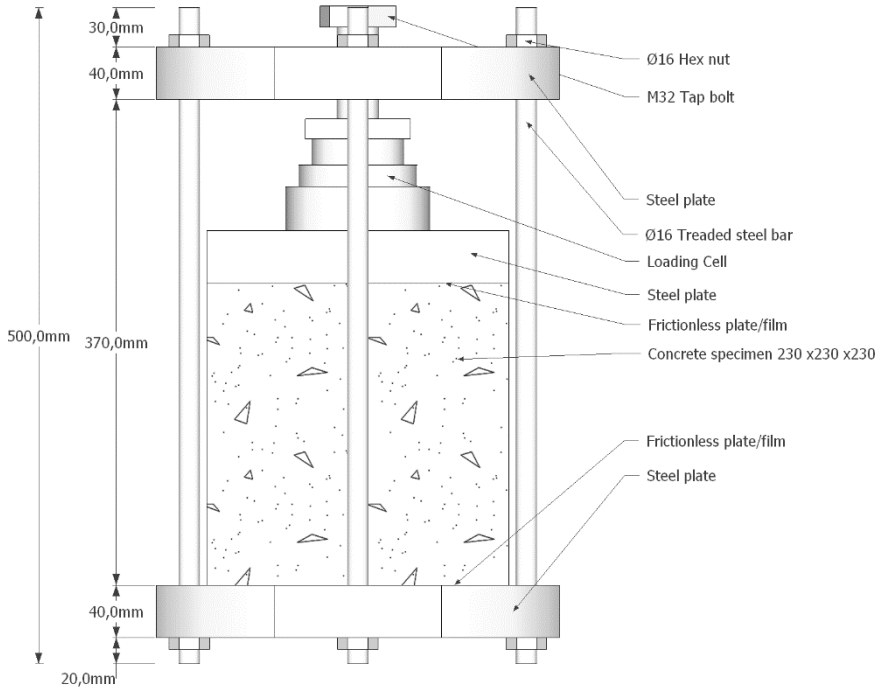

Figure 3. A sketch of the restraint set-up.

Since the restrained prims where connected to a teflon plated and steel plate on both surfaces in z-direction (restrained direction), thin steel plates were added on the same surfaces on the prisms which were free to expand. This was done to acquire equal moisture transportation in the restrained prisms and the free prisms.

A machine designed to investigate the effect of creep was used to maintain constant stress on the restrained reference prisms. The machine uses a combination of compressed gas and oil to keep a stable pressure. The accumulated pressure pushes a piston upwards, which is separated from the prism by a steel plate at the bottom, adding stress to the prism. A steel plate was added to the top between the prism and the loading cell. The loading cell was connected to a computer that displayed and logged the load. The creep machine owned by NTNU was used stationed at the concrete laboratory in a climate room keeping 20°C and 50%RH.

A reactor much simpler than the one described by RILEM[30] was built to control and keep the desired temperature of 60°C. Figure 4 shows an illustration of the reactor. It consisted of an isolated box with outer dimension of 2040 mm x 840 mm x 1500 mm. One and a half pallet topped with 50 mm isolation was used as the bottom of the reactor, making it easy to move. The rest of the box was made of two wooden plates with 50mm isolation between. To keep a temperature of 60°C, an air heater with a thermostat was installed inside the box along

with a fan that circulated the air continuously. A thermometer was installed inside the box, measuring and logging the temperature.

The reactor was placed inside a climate room keeping 38°C to lower the temperature differences and thus lower the necessary isolation required. A test run reaching and maintaining 60°C was performed prior to the start of the experiment with constant observation. This was done to make sure we could maintain 60°C in the reactor and inside the buckets, and checking that the climate room remained unaffected when the reactor reached 60°C.

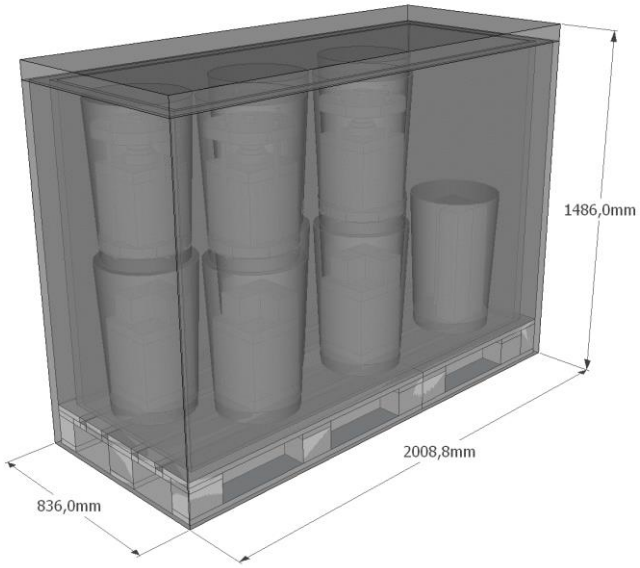

Figure 4. Reactor RILEM recommendation (figure 1 p. 102 [30]).

To obtain better control of the moisture and keeping the conditions more stable when the reactor were opened (e.g. to acquire a sample for testing), all samples to be tested on the same time was kept in separate plastic buckets with a layer of water in the bottom. The plastic buckets were similar to the ones SINTEF are using in ASR experiments at 38°C. The buckets have a height of 550 mm and a diameter of 330 mm at the bottom and 380 mm at the top and are closed with a lid at the top. Around the inner wall of the buckets a sheet of fiber cloth was glued in place to help transport water from the bottom to the top of the buckets. Inside two of the plastic buckets, the one closest to the heater and the one furthest apart from the heater, a thermometer is installed, measuring and logging the temperature. The placement of the different samples inside the containers is illustrated in figure 5. Using plastic bucket with a layer of water inside made it possible to have dry condition inside the reactor, which made it possible to build and use a much simpler reactor in this experiment compared to the one described by RILEM [30].

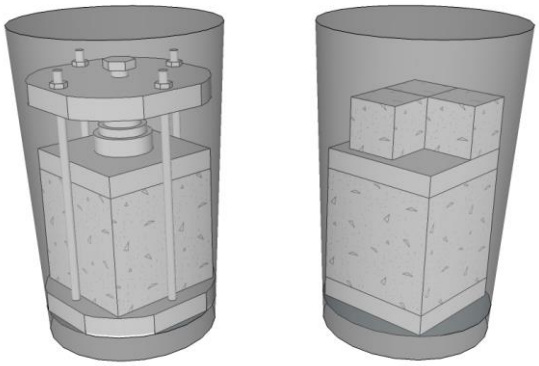

Figure 5. Storing of the different samples inside the plastic buckets.

3.3 Development over time

In order to analyze how the mechanical properties change over time, 4 different testing times have been chosen based on RILEM AAR-4.1 [30]. ASR expansion in laboratory testing seem to follow a S-curve [2]. The first testing was done when initial ASR started to develop, and the prisms started to expand. The second and third test were done in the phase with rapid ASR development. The last test was done when the AST development started to decline. Testing took place after 5, 10, 15 and 21 weeks of exposure. At each of these schedule testings, 1 prism from each of the 4 different exposure conditions (RP60, FP60, RP20 and FP20) wa s acquired. From the restrained prisms 4 cylinders were drilled out, 2 in the z-direction (restrained direction) and 2 in the y-direction (unrestrained direction). From the unrestrained prisms 2 cylinders in z-directions were drilled out. The SDT was carried out on all the 12 cylinders drilled out. In addition to the SDT, expansion measurements of all prisms were done on the prisms prior to drilling of the cylinders as well as a compressive strength test on 6 cubes, 3 reference cubes and 3 cubes exposed to accelerated ASR conditions. The tasks and schedule of the performed experiments are organized in a Gantt diagram in table 3.

Table 3. *Schedule of the planed experiment.*

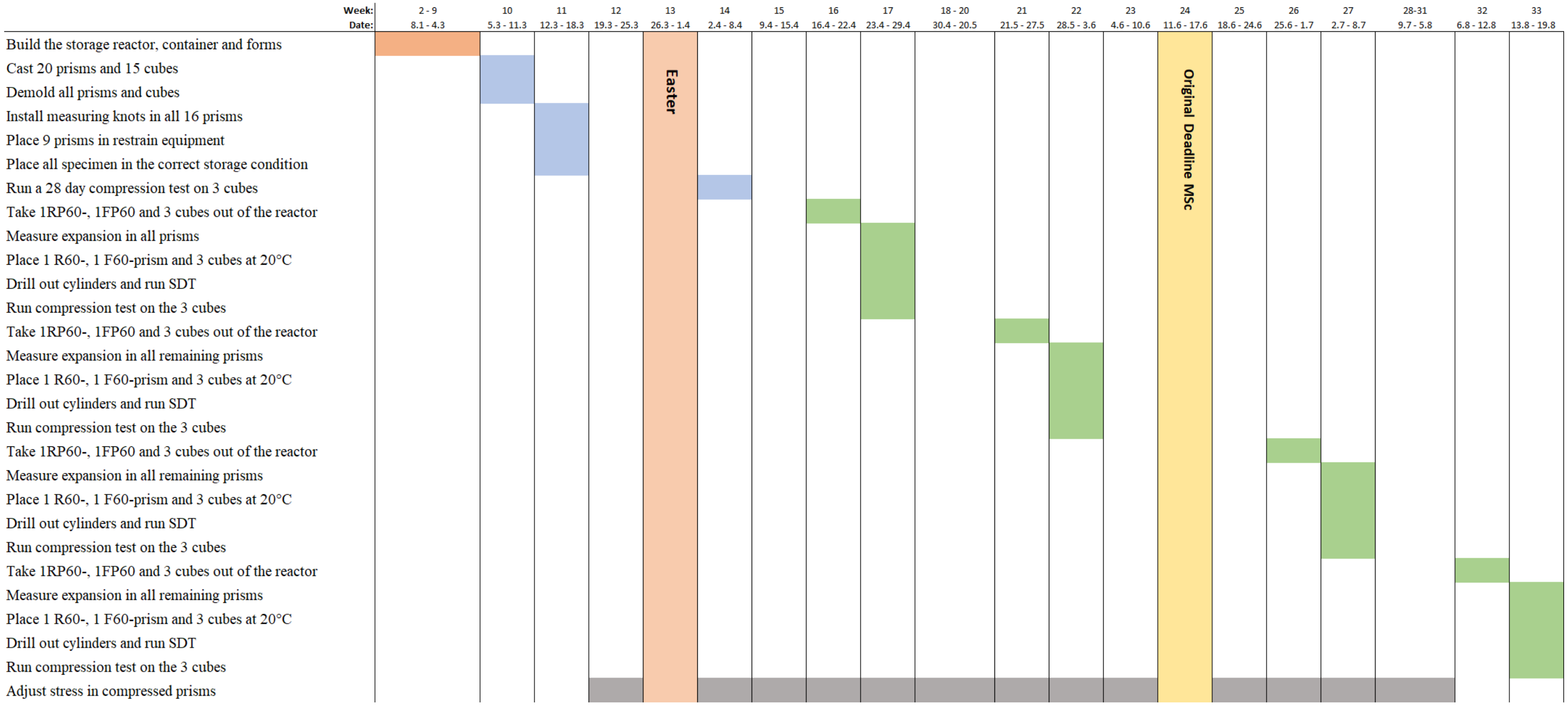

3.4 Adjusting stresses

The computer connected to the load cells made it possible to see the applied stress on the prisms. This made it possible to adjust the stress on the prisms standing in the reactor manually, by tightening or loosening the bolt in the threaded steel bars showed in figure 3. Tightening was done once a week the first 2 weeks of exposure. Then it was done once every second week the next 8 weeks of exposure. After 10 weeks the stress increased slightly due to the pressure from the expanding prisms. As the increase was minimal, loosening of the remaining prisms was done once. Tightening and loosening of the system was done as infrequent as possible, in order to minimize the effect of temperature drop from opening the reactor and taking the equipment out of the buckets. In addition, the equipment and prisms weigth about 100kg each, making the adjustment process tiresome.

The stress on the reference prisms kept in the creep machine had to be adjusted regularly throughout the experiment, as the stress slowly decreased over time. During the first weeks the stress had to be adjusted twice each day. The interval between the adjustments gradually decreased. In the end of the experiment adjustment was made once every second week.

3.5 Compressive strength

The compressive strength of the cubes and cylinders were found by inducing a compressive force with regular increases of 0.6MPa/s until the cube cracks and fail. The loading was stopped immediately after failure and the highest compressive force is noted as the compressive strength as described in the Norwegian Standard NS-EN 12390-3 [32]. The hydraulic load frame model 2031 from ToniTecknik was used to run the compressive strength test on the cubes and the cylinders were tested using a FormTest Alpha 4/B-62(SINTEF).

3.6 Work diagram

4 cylinders were marked to investigate the complete work diagram at each scheduled testing. The investigation was done by SINTEF in the concrete laboratory according to their standard procedure. The test was performed in a 5000kN compressive frame from Losenhausen.

3.7 Stiffness damage test (SDT)

To perform the SDT the cylinder was exposed to five loading/unloading cycles up to 40% of the cylinder design strength, which was calculated from the 28-day compressive strength test done on 3 cubes. The cylinder design strength was found to be 41.0 MPa by using the conversion from cube strength to cylinder strength according to NS-EN1992-1-1 [33]. This resulted in a max load of 16.4 MPa in each load cycle. Prior to the first load cycle the frame model

was started and stopped when connection to the sample was attained, at about 1.5 MPa. During the load cycles the load intensity was increased by 0.10 MPa/s until desired max load of 16.4 MPa, then the load was decreased by 0.10 MPa/s until 1.5 MPa, similar to the approach described by Sanchez et al. [18]. The maximum/minimum stress level was kept for less than 4 seconds at the top/bottom of each load cycle. The lower limit of 1.5 MPa was used to prevent the frame model from losing connection to the sample. After the five load cycles, 4 cylinders from 4 different exposure conditions were placed aside to investigate the work diagram. On the remaining 8 cylinders the standard compressive strength test was run. Controlling the start, stop, increase and decrease during the load cycles was done manually. FormTest Alpha 4/B-62(SINTEF) compressive load frame was used to perform the SDT.

3.8 Expansion

Measurement of expansion were performed similar to the procedure explained in SVV report number 465 [29].To measure the expansion two small measuring knots were installed on each end of the sample. The knots were installed approximately 200 mm apart by gluing the knots to the surface while holding them down using a reference rod, to make sure that they were close to 200 mm apart. They were installed prior to exposure, hence at 20°C. After the installation, the distances between the knots were measured and noted using a measuring rod with micrometer accuracy.

As the focus in this paper is change in mechanical properties and degree of damage, expansion measurements were only done when the specimens were taken out prior to SDT, with the assumption that the different prisms will expand equally under the same storage condition. This means that expansion in F/RP60-2, -3, -4 and -5 are assumed to reach the same expansion as the measured expansion in F/RP60-1 after 5 weeks of exposure.

An expansion measure was done right after the prisms were removed from the reactor and again after the prisms had cooled down. This was done as a control measurement and to estimate the thermal dilation. The expansion presented in the results are the expansion measured after the prisms have cooled down.

3.9 Pre SDT procedure

The restrained prisms exposed to constant stress and accelerated ASR were removed 5, 10, 15 and 20 weeks after load and conditions were applied, respectively. After the restrain was removed the expansion of the prisms were measured within 10 minutes. The first 24±2h, the prisms were stored in a climate room keeping 38°C. Then the prisms were moved and stored

minimum 48h in room temperature (20°C). The long cooling period was done to make sure the whole prisms were cooled to 20°C, not just the surface, when the expansion was measured again, as the prisms is quite large. During the cooling period the prisms were still stored in the same plastic buckets keeping the humidity very high, close to 100% RH. The prisms were kept in the plastic buckets until cutting and were only removed during the expansion measurement.

The unrestrained prisms exposed to accelerated ASR were removed from the reactor at the same time as the restrained prisms. Within 10 minutes of removal the expansion of the prisms was measured. The cooling process were the same as for the restrained prisms, 24±2h in 38°C followed by minimum 48h in 20°C while the prisms is still stored inside the same plastic buckets until cutting.

Expansion of the restrained reference prisms was measured while the prisms were restrained, then the prism were released from the stresses. The expansion measure was repeated after the release to control for the effect of releasing the stress. The prisms were stored in the same room until cutting, keeping the storing condition constant, at 50% RH and 20°C.

The unrestrained reference prisms were left as is, in room temperature, at 20°C, packed in wet linen bags under a plastic sheet, 90-100% RH, until cutting procedure took place.

3.10 Cutting procedure

Prior to drilling and cutting, the expansions were measured again and noted for all prisms prepped for cutting.

In order to run the stiffness damage test, cylinders with diameter of 95±1 mm and height of 190±1 mm had to be drilled out of the prisms, giving a height:diameter relation of approximately 2:1. The cylinders were cut to a height of 193±1mm at the first two scheduled testings, due to a communication error. However, the height:diameter ratio were still approximately 2. The drilling process was done in the manner illustrated in step one in figure 6. The drilling

process were done in water making every cylinder almost equally wet and fully saturated. The drilled-out cylinders were packed in plastic sheet to keep the cylinders moist.

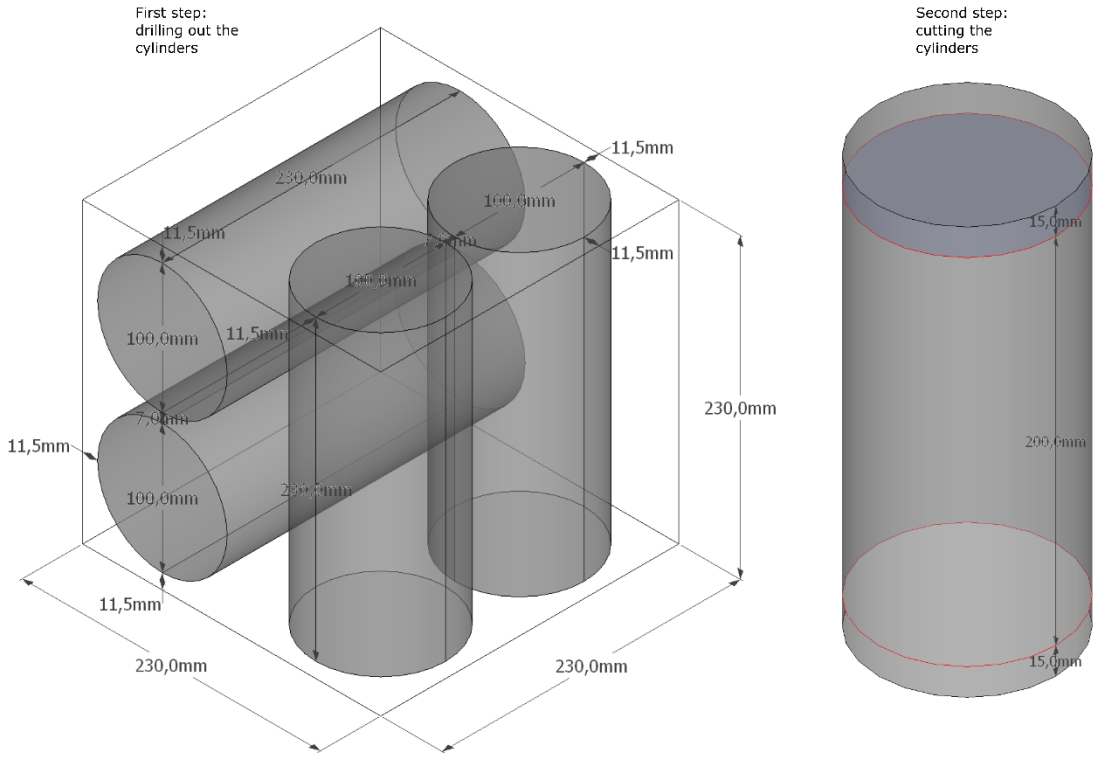

Figure 6. Show the two steps of the drilling and cutting and approximate dimensions of the cylinders.

After 24h the cylinders were cut and grinded into the desired height of 190mm. This was done by cutting approximately 20 mm on each side, which ensured that the cylinder was taken from the middle of the prism. The grinded cylinders were packed in plastic sheet, keeping the moisture and preventing shrinkage until testing. Prior to testing the cylinders were weighed in air and water and surface dried using a paper towel. In total 32 cylinders were drilled out to perform SDT followed by a compressive strength test. On 16 cylinders SDT were performed followed by an investigation of the work diagram. The measured diameter, height, air density and water density are presented in appendix B.

3.11 Output parameters from SDT

Over the years, different outcome parameters from the SDT have been presented. In this paper the indices SDI, PDI and NLI as described by Sanchez et al. [26,27] are used to analyze the SDT. In addition to the 3 indices, elastic modulus was calculated from the SDT, in a similar way as described by Chrisp et al. [24]. Calculations of the 3 indices and elastic modulus were done in excel in the following manner:

- SDI: The area under the upward curve and downward curve in each load cycle is calculated using trapezoid rule. SI is then given by the area under upward curve minus the area under the downward curve in a load cycle. SI + SII is given by the area under the upward curve of a load cycle. SDI is then defined as the sum of SI areas over the five load cycles divided by the sum of SI + SII over the five load cycles, as shown in formula 2:

$$SDI = \frac{\sum_{i=1}^{5} SI_i}{\sum_{i=1}^{5} (SI_i + SII_i)} \qquad (2)$$

- PDI: DI = last logged strain value – first logged strain value, DII = Strain logged at the top of last load cycle – last logged strain value.
- NLI: calculated as shown in formula 3:

$$NLI = \frac{\sigma_{hmx}/\epsilon_{hmx}}{\sigma_{mx}/\epsilon_{mx}} \qquad (3)$$

σ_{hmx}: Stress at half of the maximum load level in the first load cycle

ϵ_{hmx}: Strains at half of the maximum load level in the first load cycle

σ_{mx}: Maximum stress in the first cycle

ϵ_{mx}: Strains at maximum stress in the first load cycle

- Elastic modulus: Average of the slope of 3 different line drawn from start of load cycle 2, 3 and 4 to top of load cycle 2, 3, and 4, respectively, as shown in formula 4.

$$E_c = \frac{\sum_{i=2}^{4} \sigma_{i\_top} - \sigma_{i\_st}/\epsilon_{i\_top} - \epsilon_{i\_st}}{3} \qquad (4)$$

E_c: Elastic modulus

σ_{i_top}: Stress at the top of load cycle i

σ_{i_st}: Stress at the start of load cycle i

ϵ_{i_top}: Strain at the top of load cycle i

ϵ_{i_st}: Strain at the start of load cycle i

- Estimating initial elastic modulus: Estimated by the slope of a line drawn from the top of last load cycle to a point 2.5MPa under the top on the unloading curve of the last load cycle

The described approach to calculate the SDI value shown above, was obtained after consulting directly with Leandro Sanchez (Assistant Professor at university Ottawa) late in the study. Our initial calculated values differed a lot compared to his values, they were about 3-4 times higher, still the SI area and PDI were in the same specter as reported by Sanchez. The first SDI values, from now on called alternative SDI (SD_{alt}), was calculated in the following manner:

- Alternative SDI: Calculate SI and SII in the same way as already described. However, form the Articles presented by Sanchez our interpretation was to divide SI by SI + SII for each load cycle and then sum the resulting factors, as shown in formula 5:

$$SDI_{alt} = \sum_{i=1}^{5} \frac{SI_i}{(SI_i + SII_i)} \qquad (5)$$

4 Results

In this chapter the result from the expansion measurement, the compressive test, the SDT, the calculated indices and the elastic modulus from the SDT will be presented. All values presented are the average of two calculated values, except for the expansion measurement, the cube compressive strength test and when faults occurred, making a value unusable. The expansion measurement and cube compressive strength test were done three times and the average value is presented. An overview of the measured compressive strength, elastic modulus, SDI, PDI, NLI and SDI_{alt} is presented in Appendix C.

4.1 Expansion

The expansion in x-direction is shown in figure 7A, y-direction in figure 7B and z-direction in figure 7C. Z-direction corresponds to the load direction. The total volumetric expansion in the free prisms and the restrained prisms exposed to accelerated ASR conditions are shown in figure 7D. The measured expansion at different times are taken from different prisms, which means that the development displayed are not the true development of specific samples, although an indication of the development.

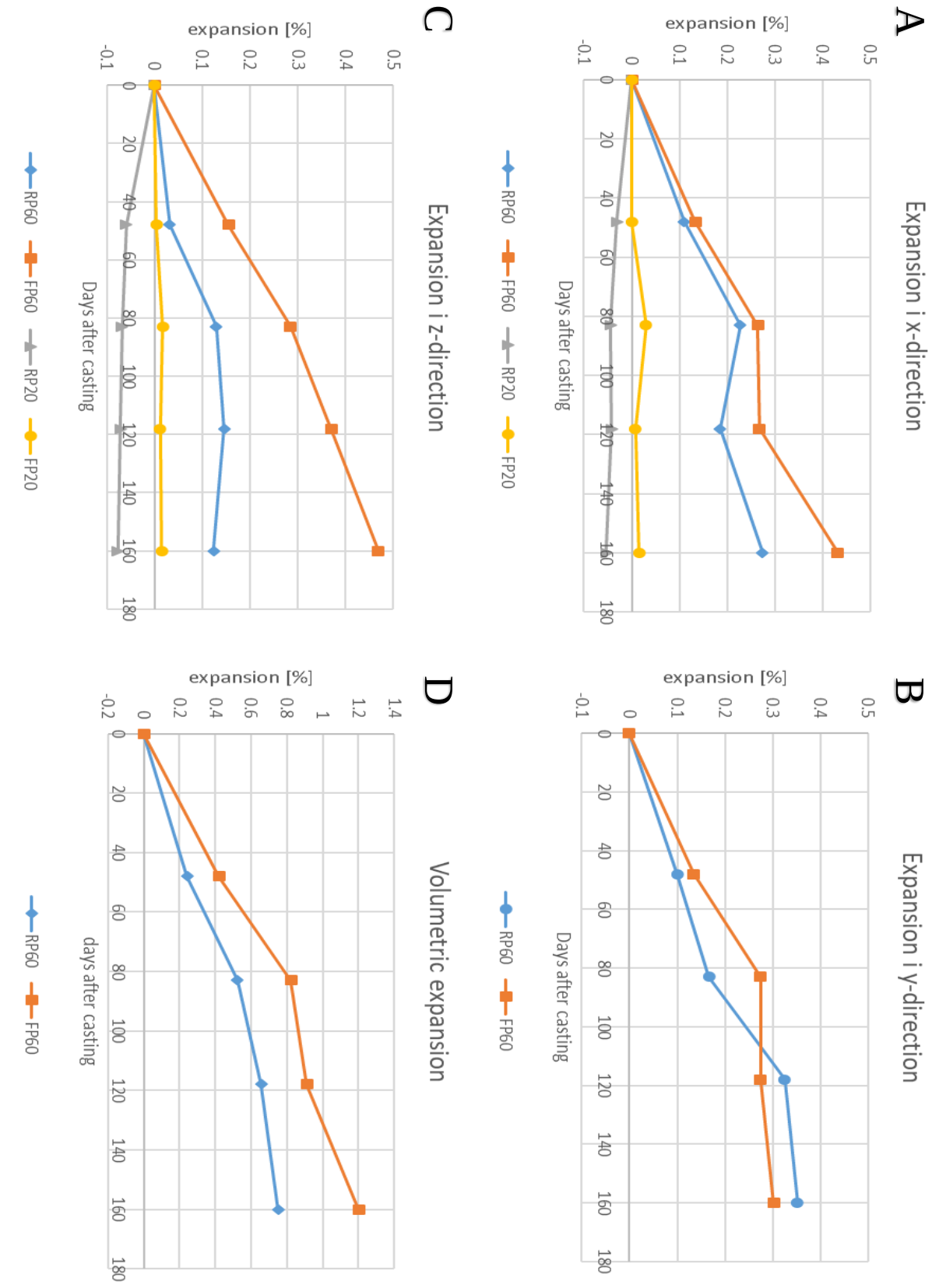

Figure 7. A: expansions in x-direction, B: expansion in y-direction, C: expansion in z-direction and D: show volumetric expansion

4.2 Stiffness damage test

Figure 8A-H show a representative selection of the stress-strain curve obtained during the stiffness damage test, and displays increasing expansion from 0.0% in A to 0.468% in H. When comparing the stress-strain curve at different expansion levels, there is a clear relation between increased expansion and plastic deformation, and thus the total energy dissipated.

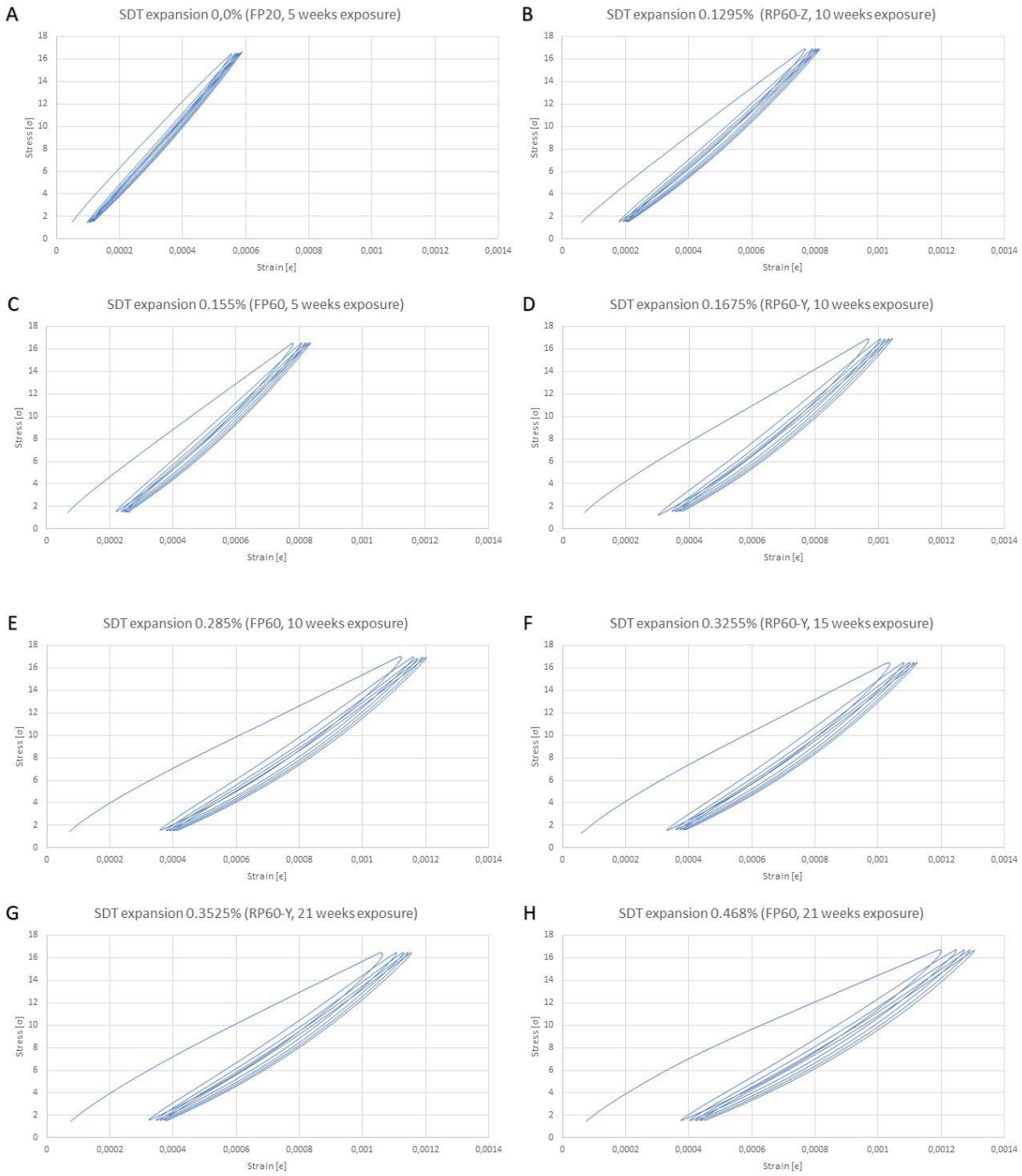

Figure 8. A-H: A selection of stiffness damage test curves from different level of expansion.

4.3 Elastic modulus

Figure 9 shows the development of elastic modulus over time in terms of days after casting. The range of values calculated is indicated by the error bars. The figure shows a concave reduction of the elastic modulus in all ASR affected samples, while the elastic modulus in the reference prisms are constants during the experiment. Less reduction of the elastic modulus can be spotted in the restrained direction (z-direction).

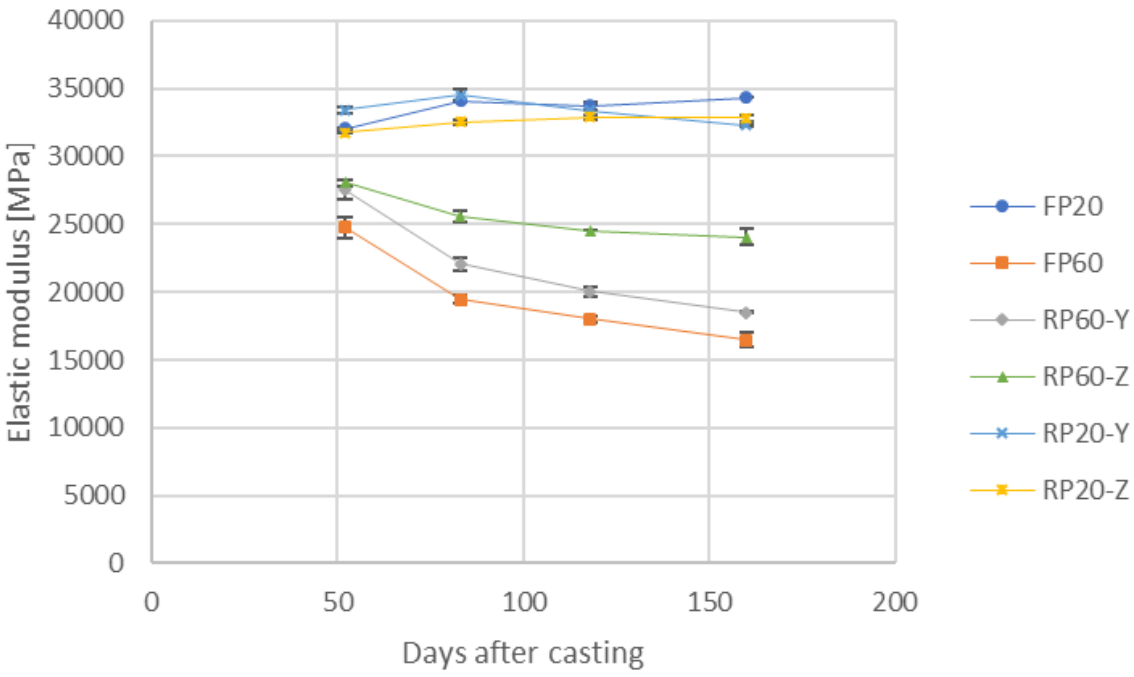

Figure 9. Elastic modulus plotted against days after casting

Elastic modulus reduction plotted against the level of expansion is shown in figure 10A/B with a fitted linear/logarithmic trend curve, respectively. This shows that the relation between elastic modulus reduction and increasing expansion can be described by both a linear function and a logarithmic function, with strong correlation in both cases. The reduction displayed is relative to the average elastic modulus measure in all reference prisms. The biggest reduction in elastic modulus occurred in the samples and direction with the largest expansion. The different colors and markers relate the points to the different storage conditions. This shows that the reduction seems to be dependent on the level of expansion and independent of the storage conditions.

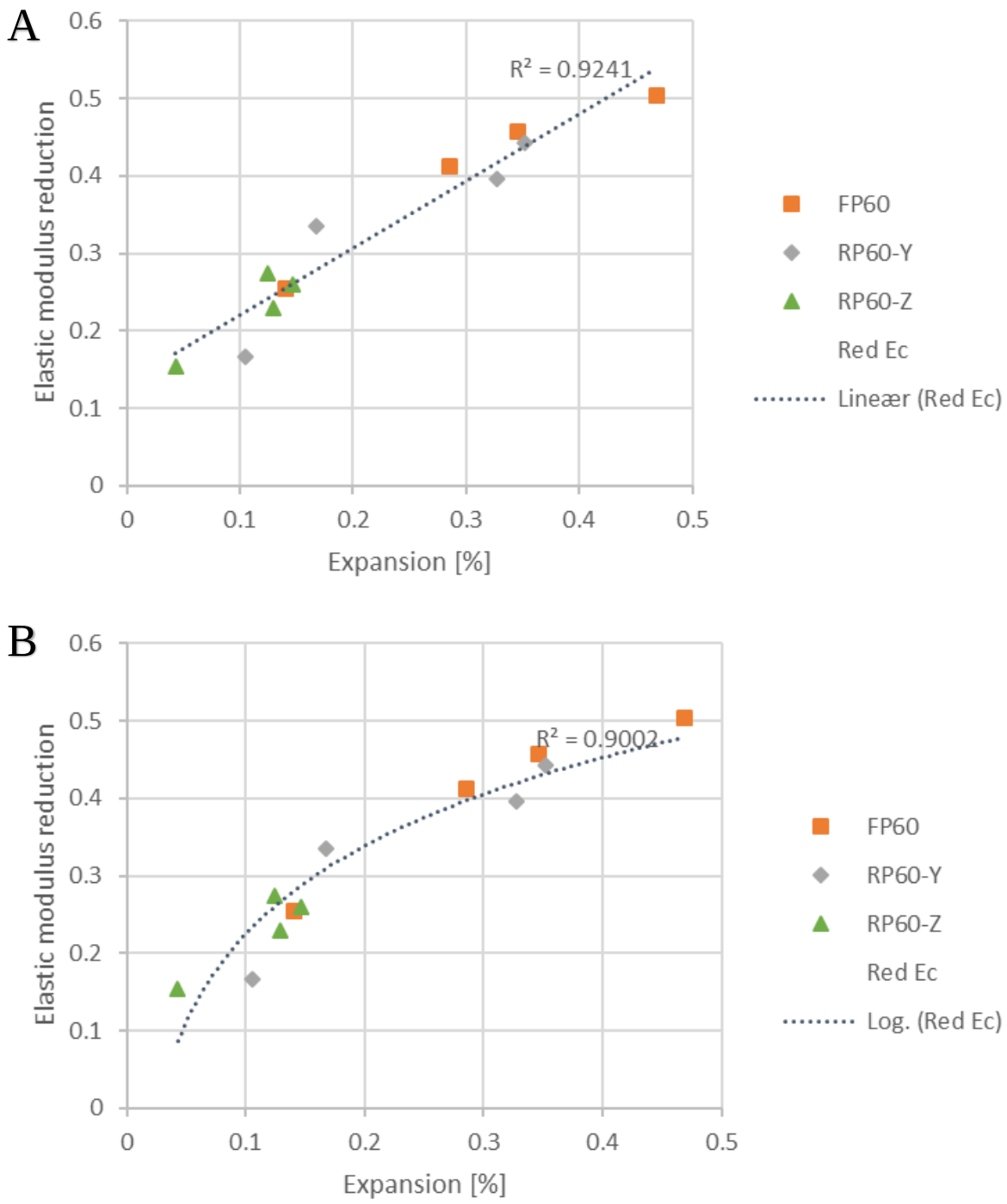

Figure 10. A/B: Elastic modulus reduction with respect to expansion with a fitted linear/logarithmic trend curve, respectively.

The estimated initial elastic modulus in the ASR affected cylinders are presented in table 4. The estimated initial elastic modulus of the free prism underestimated the initial elastic modulus with about 4000 MPa. The estimate initial elastic modulus for the restrained prisms are close to the measured elastic modulus in the reference prisms.

Table 4. Estimated initial elastic modulus

Sample	Estimated initial elastic modulus				
	week 5	week 10	week 15	week 21	Average
FP60	34073	28602	27510	26840	
	33412	29387	28797	26120	29343
RP60-Y	36463	32364	29493	28452	
	34484	31636	30192	28771	31482
RP60-Z	35008	32798	31322	32348	
	34511	33543	32295	31495	32915
Average	34659	31388	29935	29004	31247

4.4 Compressive strength

The compressive strength measured from the 100 x 100 x 100 mm cubes are presented in figure 11. The test results at 48 days after casting shows a significant increase in strength on all 3 cubes stored in accelerated ASR conditions and the 3 reference cubes stored at 20°C compared to the strength in reference cubes after 30 days of curing. The strength increase is larger at the accelerated conditions than at the reference conditions. However, a reduction in strength is apparent in the cubes exposed to accelerated ASR at the 83 days test compared to the reference cubes. Further compressive strength testing, at 113 and 160 days after casting, showed almost constant compressive strength in ASR affected cubes, while the strength of the reference cubes continued to increase.

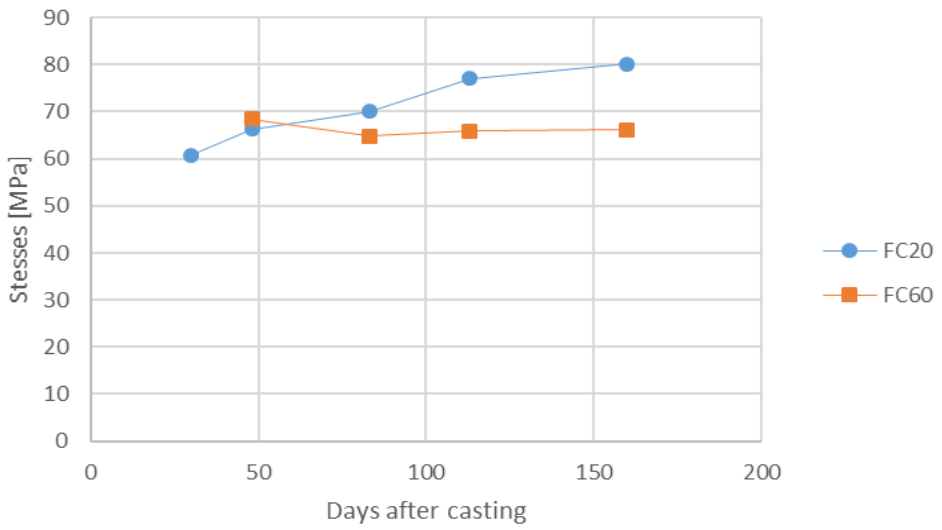

Figure 11. Cube compressive strength against days after casting.

The cylinder compressive strength is presented in figure 12. The first test, 48 days after casting, show larger compressive strength in the cylinders corresponding to larger expansion levels in FP60 and RP60-Y. A lower compressive strength can be seen in restrained direction compared to unrestrained direction throughout the experiment, both in ASR affected cylinders and reference cylinders. The difference is significant at 48 and 84 days after casting and insignificant at 114 and 160 days after casting. The 84 days testing of the cylinder show almost the same compressive strength in all cylinders tested except for RP60-Y and RP20-Z. The first is 5MPa higher and the latter is 6 MPa lower. First after 114 days since casting, a reduction in the ASR affected cylinder compared to the reference cylinder drilled from the free prisms (FP60 and FP20) can be seen.

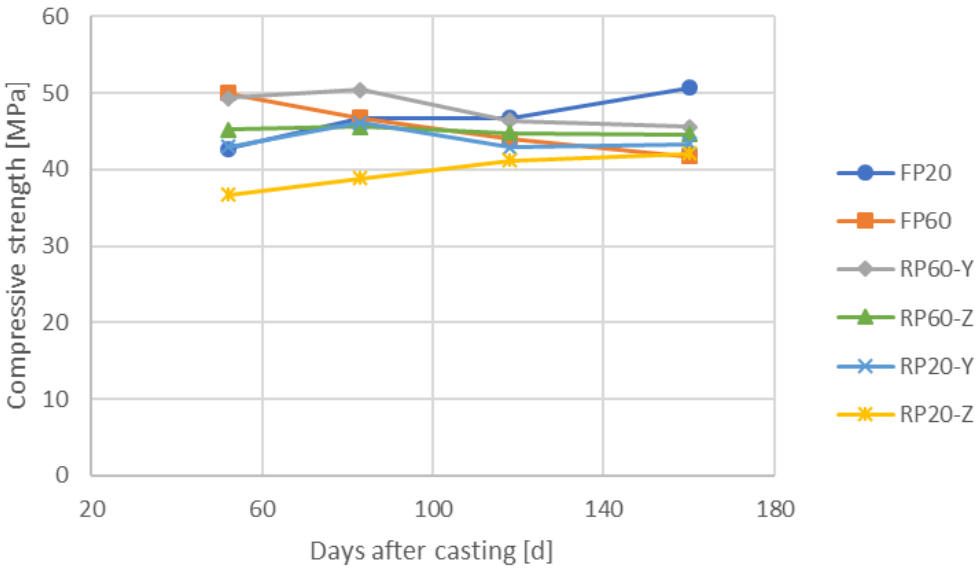

Figure 12. Cylinder compressive strength against days after casting.

In figure 13 the compressive strength of the cylinders is plotted against the degree of expansion. A gradual reduction in compressive strength with increasing expansion is distinguishable from the linear tend line drawn considering only the measured compressive strength in cylinders with positive expansion.

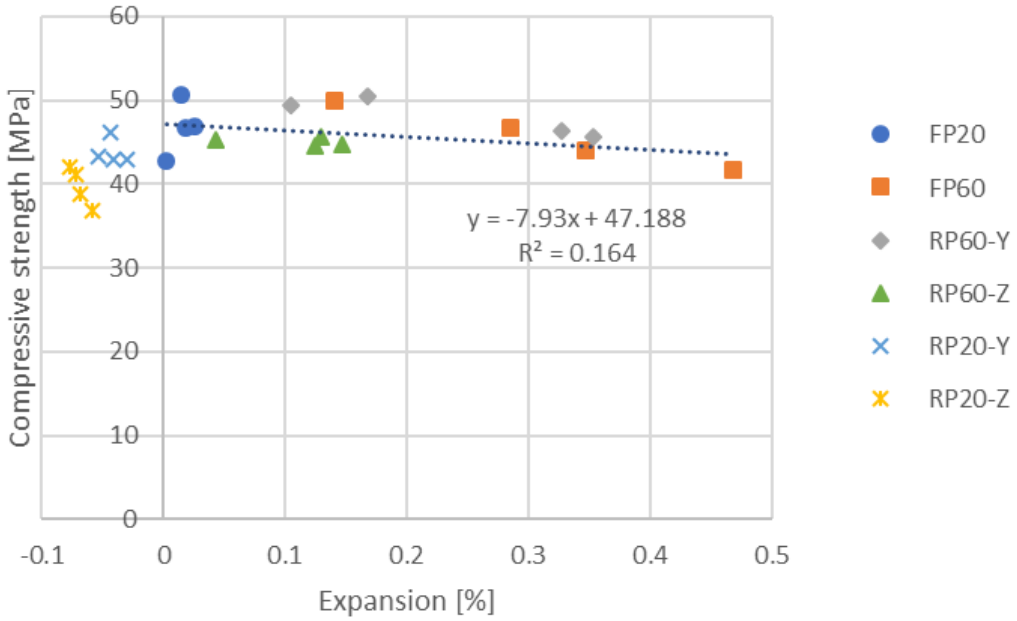

Figure 13. compressive strength plotted against expansion, with a linear trend line considering only the strength measure in cylinders with positive expansion.

4.5 SDT damage indices

Figure 14 present the relationship between stiffness damage index (SDI) and expansion with a fitted logarithmic trend curve. This trend line show that the relation between calculated SDI and expansion are close to a logarithmic function with an R^2 of 0.7331. The range of calculated values are indicated by error bars.

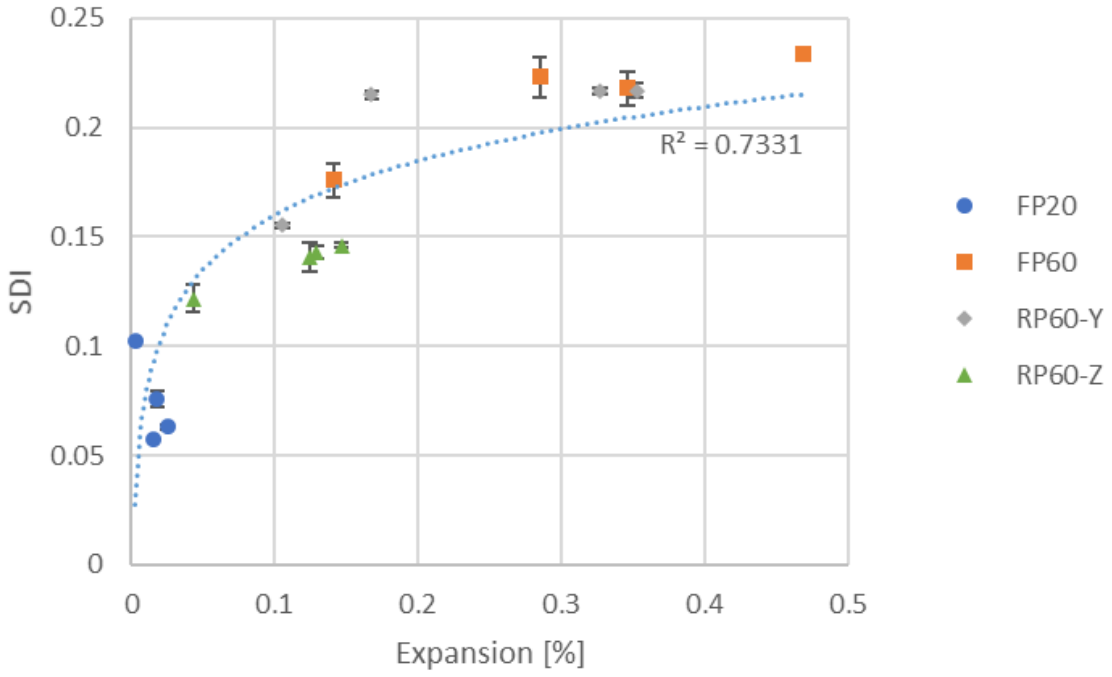

Figure 14. SDI plotted against expansion with a plotted linear trend curve.

Figure 15 shows the plastic deformation index (PDI) and expansion with a fitted logarithmic trend curve. This trend line also fits good to a logarithmic curve with an R^2 of 0.686. The range of values calculated in the 2 cylinders drilled from one prism in the same direction are indicated by error bars. An interesting observation to note is that every SDI and PDI calculated from cylinder taken in restrained direction are located under the trend line.

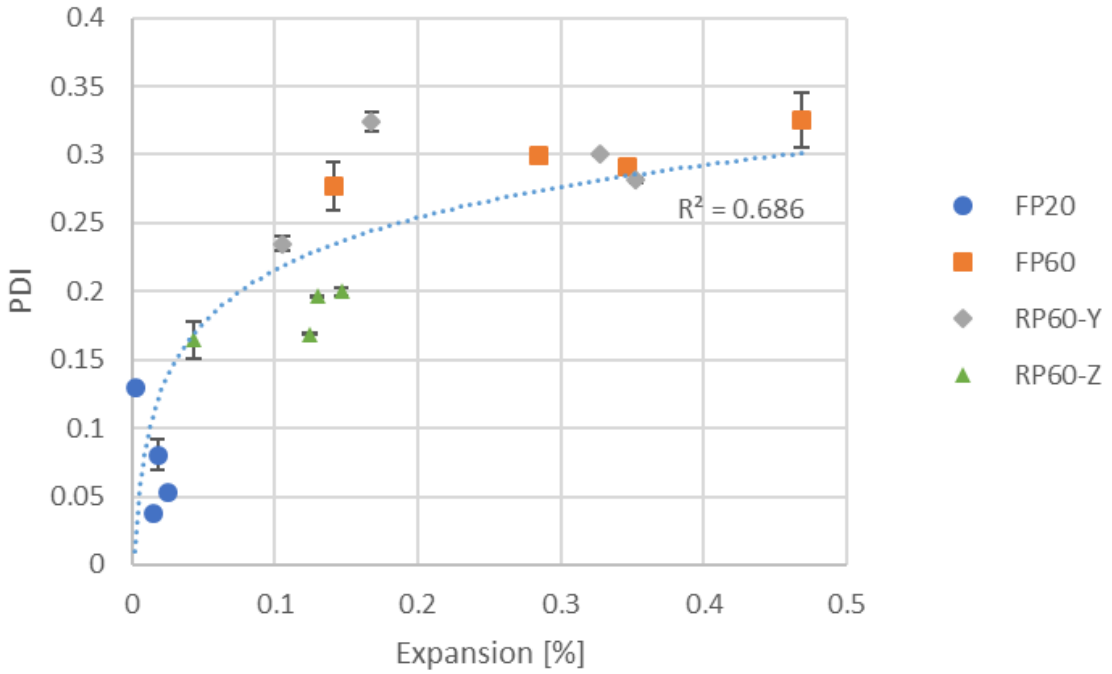

Figure 15. PDI plotted against expansion with a plotted linear trend curve.

The third index denoted NLI plotted against expansion is shown in figure 16 with a linear trend line based only on the positive expansion values. The line is a good fit to the relation between NLI and expansion, with an R^2 of 0.8602. The range of values calculated are indicated by error bars. An overall low NLI are reported in cylinders extracted from the restrained direction of the ASR affected prisms.

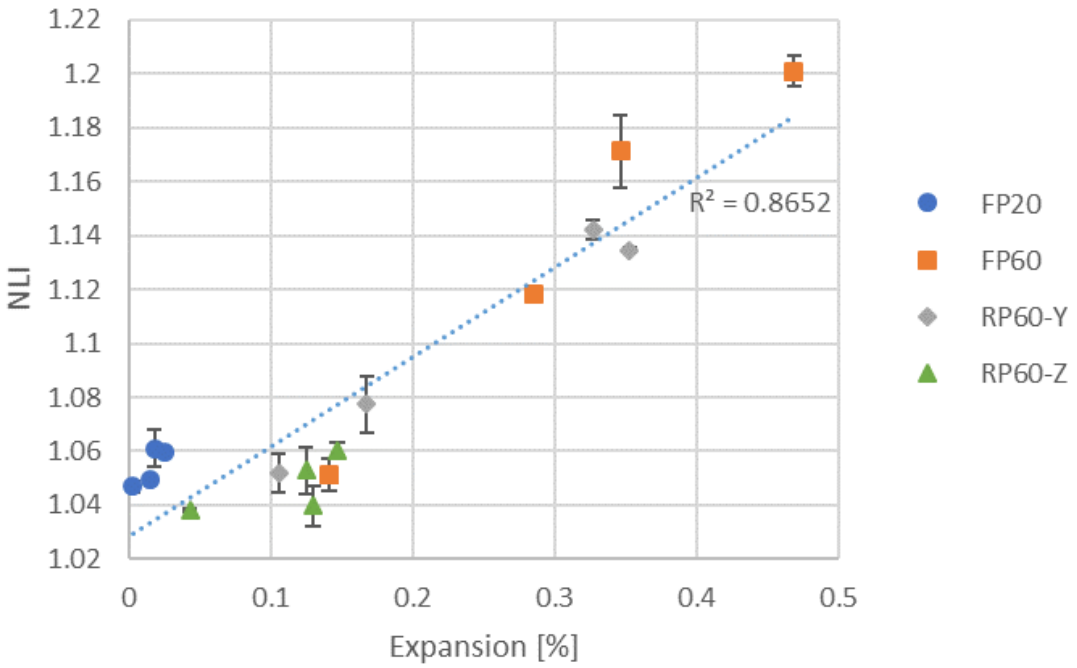

Figure 16. NLI plotted against expansion with a linear trend curve.

The alternative SDI calculate are as expected following the same relations as the ordinary SDI with respect to expansion, hence the relation follows a logarithmic function. The calculated alternative SDI are shown in table 4 and plotted against expansion in figure 17, with a logarithmic trend curve.

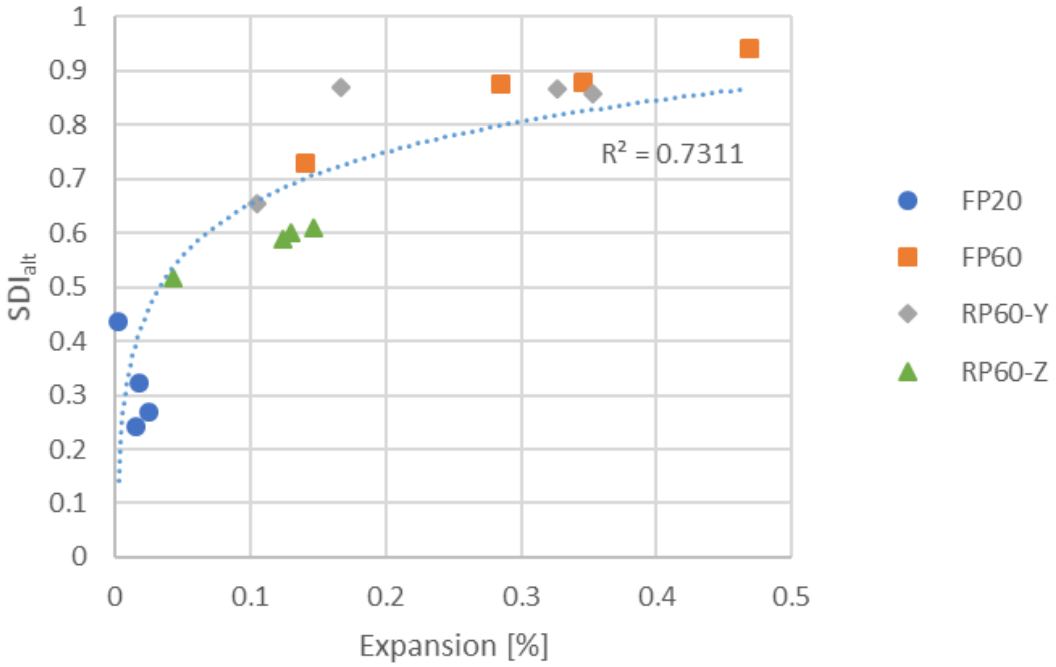

Figure 17. Alternative SDI plotted against expansion.

4.6 Work diagram

Figure 18 A-D shows the work diagram achieved from the 4 cylinders set aside after the SDT run after 5, 10, 15 and 21 weeks of exposure to accelerated ASR conditions or reference conditions. Figure 18A and B show the resulting work diagram of cylinders attained from FP20, FP60, RP60-Y and RP60-Z prisms. Figure 18C and D show the resulting work diagram from cylinders attained form RP20-Y, RP20-Z, RP60-Y and RP60-Z prisms. The ASR affected cylinder seem, when comparing the 4 different plots, to become more ductile with increasing level of ASR development. This coincide well with the larger elastic modulus reduction and almost no compressive strength reduction measured with increasing expansion.

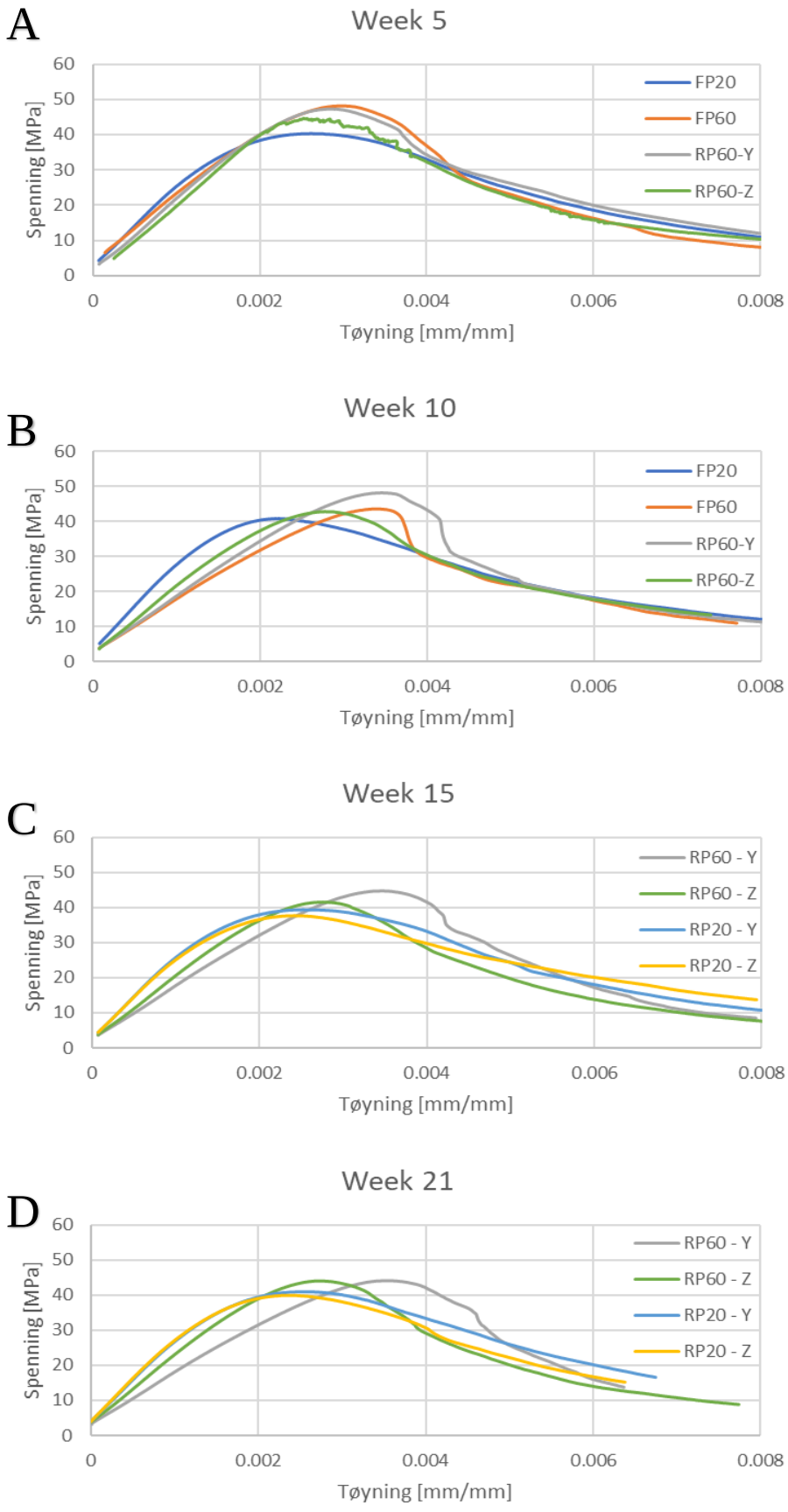

Figure 18. A-D: Work diagram atteined after 5, 10, 15 and 21 weeks, respectivly.

5 Discussion

The chapter starts by discussing the changes in expansion, mechanical properties and degree of damage occurring during the experiment. This is followed by a discussion about SDT as a tool to predict expansion development and changes in mechanical properties.

5.1 Expansion

The expansion measurements were only taken before a prism was applied for testing. In addition, the expansion measurement in one direction is only taken from one place on the surface of the prisms. To get a more accurate expansion measurement, it should be measured at different places on the surface. This means that the graphs in figure 7A-D are not describing the continuous expansion development. However, the graphs still give an indication of how far the ASR has developed, and the indices, compressive strength and elastic modulus reduction are compared to the actual expansion in the cylinder.

The measured expansion is somewhat higher than our estimate during the preparation of the experiment. This is not unexpected as most experiments with the same concrete mix is stored at 38°C as opposed to our sample, which was stored at 60°C. The difference in temperature is likely the explanation for the underestimation. This emphasize a lack of experience with ASR testing at 60°C. ASR testing at 60°C is beneficial with respect to the time aspect, as the same expansion level reached after 15 weeks of exposure are achieved after about 52 weeks storage at 38°C. The 60°C ASR test is possibly preferential if e.g. one would like to assess many different concrete mixes. However, the effects from high temperature on the gel and the related concrete properties are still uncertain and further testing should be conducted.

When comparing the measured expansion with the studies of Berra et al. [7] and Gautam et al. [8], our study showed more final expansion in restrained direction with similar compressive stress. More expansion in unrestrained direction compared to the expansion measured in free prisms was reported in both studies. This points toward a transfer of expansion from restrained direction to unrestrained direction. A transfer of expansion is a suggested explanation for the similar volumetric expansion reported, meaning the sum of expansion in all direction, in all prisms, independent of restrain. Contrary to the studies of Berra et al. [7] and Gautam et al. [8], a lower volumetric expansion in restrained prisms compared to free prisms is found in our study, and a similar level of expansion in unrestrained direction and free prism is also found in our study. This suggests that no transfer of expansion occur. The difference could be

explained by use of different concrete mix and more accelerated conditions. There is a difference between our procedure of measuring expansion and the one used by Gautam et al. [8] and Berra et al. [7]. The expansion measurement in our case was done after the stress was removed while they performed the measurement when the constant stress was still applied. This means that the reported expansion in their case contains a contraction because of compressive stress in addition to the internal loading due to ASR. The elastic release expansion due to unloading included in our case, can be estimated by Hooke's law. This gives a contribution to the measured expansion between 0.01% to 0.015% in restrained direction, depending on the elastic modulus used, initial or reduced. The effect of external stress would therefore not change the measure volumetric expansion much, as the long-term volumetric expansion measured in our case is 1.2% in the free prism and 0.75% in the restrained prism. The long-term volumetric expansion reported in Gautam et al. [8] study is 0.47% +- 0.01% in both the free and the restrained sample. This means that our samples had a much larger level of expansion. The overall larger expansion during our experiment could explain the higher expansion in restrained direction with similar constant compressive stress compared to Gautam et al. [8], and the internal load due to ASR is likely larger in our study. The effect of internal load is unknown. The large difference in volumetric expansion in restrained prism and free prism, and the lower expansion measured in both unrestrained directions, in all restrained prisms, except for 2 values, compared to the free prism. This points to no transfer of expansion in our study.

5.2 Elastic modulus

As previous studies have already shown [18–20,26], the elastic modulus is clearly affected by ASR. The elastic modulus reduction is a good fit to a linear function with increasing expansion as shown in Figure 10A, with a linear regression line with a R^2 of 0.9241. This suggests that the cylinders drilled in the restrained (z-) direction should show less decrease in elastic modulus compared to the cylinders drilled in the unrestrained (y-) direction, as was the case in all restrained prisms stored inside the reactor. The reference prisms showed no reduction, as expected. The stress-strain curves in Figure 18A-D shows that the ASR affected samples with increased reduction of elastic modulus displays more deformation before failure load is reached, indicating a more ductile behavior in ASR affected concrete.

The strong linear correlation between elastic modulus and expansion shown in figure 10A, points to elastic modulus as an interesting parameter when assessing ASR damaged structure. It suggests that elastic modulus reduction is dependent on the level of expansion and can be used to estimate the expansion. Despite elastic modulus being individual for each different

concrete mix, Sanchez et al. [27] showed that the reduction in elastic modulus had a similar correlation for 20 different concrete mixes composed of 13 different aggregates. The range of elastic modulus reduction calculated (indicated by yellow dotted lines) and our measured elastic modulus reduction is shown in figure 19. This suggests that the correlation between degree of elastic modulus reduction and expansion is to a certain degree universal for all concrete mixes. This, together with the seemingly accurate estimation of initial elastic modulus, especially in the restrained samples, opens for a possibility to estimate the expansion using elastic modulus from SDT and the estimated initial elastic modulus.

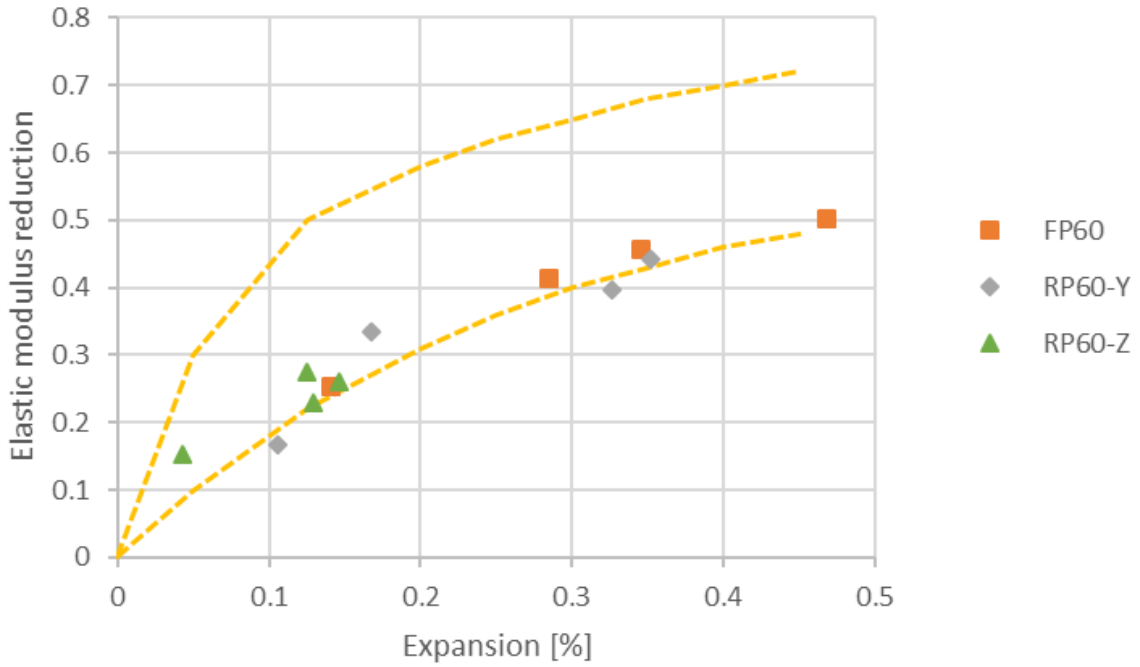

Figure 19. Elastic modulus reduction against expansion and the range of elastic modulus reduction found by Sanchez et al. [27], upper and lower values are indicated by the yellow dotted lines.

5.3 Compressive strength

Unlike elastic modulus and the SDT-indices SDI, PDI and NLI, no correlation is apparent between compressive strength and expansion level, which can be seen in figure 12. The higher compressive strength measured in the prisms exposed to highly accelerated ASR condition is unexpected, as both Sanchez et al. [26] and Jones and Clark. [10] reported a loss in compressive strength after long term exposure to accelerated ASR conditions. It was showed by Balendran et al. [14] that higher curing temperature than 42°C had a small negative impact on compressive strength after 28-days of curing compared to samples cured at 27°C when using ordinary Portland cement. This means that high curing temperature have a negative impact on the long-term compressive strength development. This is contrary to the high compressive

strength measured in the cylinders drilled from FP60 and RP60 at the first testing. However, similar result has been reported by others e.g. Sanchez et al. [26] and Marzouk et al. [20].

Brooks et al. [17] showed an increase in compressive strength in samples exposed to low RH compared to high RH. Based on this, a higher compressive strength was expected in the reference prisms standing in the creep machine compared to the reference prisms stored wet packed in plastic sheet. Another factor affecting the compressive test is the moisture level of the cylinder when tested. The reference prisms in restrain were kept at about 50% RH, while the other prisms where stored at close to 100% RH. During the cutting procedure, the cylinders is saturated with water, which contributes to reducing the differences. Nonetheless, not even a fully saturation of the previously dried cylinder would completely reverse the drying effect during storage as showed by Brooks et al. [17] when investigating and reporting change in bulk modulus of dry, wet and rewetted samples. The change in compressive strength was not investigated. However, change in modulus means a change in mechanical properties and hence a possible change in compressive strength. I addition, Shoukry et al. [16] showed that dry samples had higher compressive strength than wet samples in an investigation of the effect different temperature and humidity at time of testing had on the mechanical properties on tested specimen. This suggests that the reference cylinders drilled from the restrained reference prisms, which should be drier compared to the other cylinders, will display higher compressive strength. Contrary to both factors, a lower compressive strength was measured in the cylinders attained from the restrained reference prisms.

Barbosa et al. [19] reported a significantly lower compressive strength perpendicular to cracks than parallel to cracks. The higher expansion in unrestrained direction should partly align the micro cracks in restrained direction. According to the result presented by Barbosa et al. [19] should the cylinders drilled parallel to the restraints. Contrary to this, lower compressive strength was found in the restrained direction compared to the unrestrained direction. This difference could partly be explained by the presence of both macro and micro cracks in their study, while in our case only micro cracks are present. In addition to the alignment of cracks, concrete exposed to constant stress starts to creep, which further influence the measured compressive strength. Brooks et al. [17] reported more creep in specimen stored dry versus specimen stored wet. This means that our reference prisms stored with constant stress in the creep machine are most likely displaying higher levels of creep compared to the prisms stored with constant stress in the reactor. This assumption is not possible to check, as creep was only measured in the reference prisms. Unfortunately, this measure is not directly transferable to

the ASR affected prisms as the humidity conditions are different. Creep and small continuous constant compressive stress are reported to have a positive effect on the compressive strength due to an adaptation effect by Bazant and Kim. [34]. The lower compressive strength reported parallel to the load direction in both the prisms stored inside the reactor and the reference prisms stored in the creep machine are therefore unexpected and the reason for this effect is not clear according to the literature. Casting direction could potentially influence the result. Nevertheless, in our case the casting direction is along the x-direction while the cylinders are drilled along the y-direction and the z-direction (restrained direction). Casting direction should therefore have minimal effect on the compressive strength.

The stiffness damage test proved to be non-destructive even when using maximum load level of 40% of the 28-days compressive strength by Sanchez et al. [18], running compressive tests on sample before and after SDT. SDT impact on measured compressive strength should therefore be insignificant. However, plastic deformation occurs, energy is dissipated performing the test, and Sanchez et al. [18] only showed that the test was non-destructive for two concrete mixes. The concrete mix used in this paper can be more affected by the SDT. To get an indication of possible effects from measuring the compressive strength after the SDT, 4 extra cylinders, 2 references and 2 ASR affected, was drilled from the free prisms and tested to failure without performing SDT. The control executed showed incremental lower compressive strength in all the samples tested without SDT confirming Sanchez et al. [18] statement that SDT is a non-destructive test.

When considering the negative effect high curing temperature and high humidity could have on the compressive strength, as Balendran et al. [14] reported. The result presented in this paper along with the reported result by Sanchez et al. [18] and Marzouk et al. [20] suggests a possible positive effect on compressive strength in the early development of accelerated ASR. Sanchez et al. [18] mentioned 0.1% expansion as the tipping point for the start of the decrease of the compressive strength. Our results yield a value closer to 0.2%, A postulated reason for the positive effect on the compressive strength is that the alkali-silica gel produced, at high curing temperature, makes the concrete less porous, by filling pores and patching internal cracks, resulting in a more even stress distribution though the cross section. Making the concrete appear as more hydrated.

On the other hand, Swamy and Asali [35] and Ahmed et al. [36] showed no increase in compressive strength when using accelerated ASR conditions, instead a small decrease was reported in both studies. The scattered and unclear compressive strength measured in our experiment supports the proposal that compressive strength is a poor parameter to consider when characterizing ASR damage. The change in compressive strength due to accelerated ASR is highly affected by concrete mix used and the storage conditions.

5.4 Degree of damage

The analyses of the SDT gives a clear indication of the importance of the orientation of the restraint, as the restrained direction show less degree of damage both with respect to SDI, PDI and NLI. In addition to the lower index-values, higher elastic modulus is found in the loading direction. All measured values point towards a lower degree of damage, except the lower compressive strength measured in the restrained direction. However, the reduction is apparent in both the ASR affected prisms and the reference prisms. This suggests that it is not an effect of ASR.

When comparing our results with Sanchez et al. [26], most factors like SDI, PDI, NLI and elastic modulus are quite similar and show the same trends. This reinforces the proposal that SDT has the ability to estimate the degree of damage in concrete, using the indices described and the elastic modulus. In turn this could be used to predict e.g. expansion and compressive strength reduction. The SDI and PDI values calculated from the present investigation are plotted against the range of values calculated by Sanchez et al. [27], in their assessment of 20 different concrete mixes, the upper and lower limit is expressed by 2 yellow dotted lines in figure 19A-B.

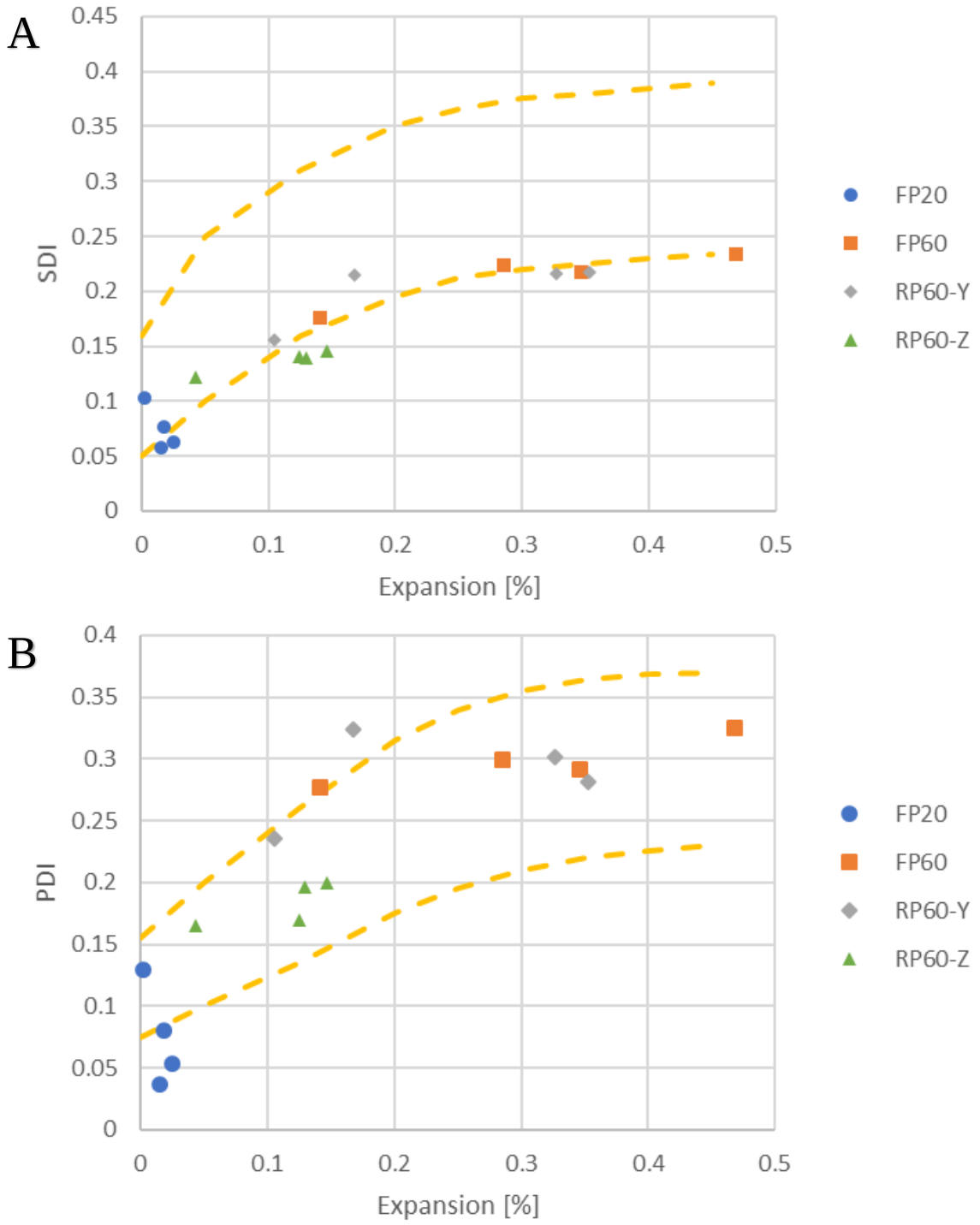

Figure 20. A: Compares SDI with the range of SDI, expressed by the yellow dotted lines, calculated by Sanchez et al. [27] B: compares the PDI with the range of PDI, expressed by the yellow dotted lines, calculated by Sanchez et al [27].

Most of the plotted values fit between the two yellow lines in figure 20A and 20B. However, the PDI values seem to be more scattered than the SDI values, pointing to SDI as the best parameter. This coincide with the higher R^2 for the logarithmic trend line plotted for SDI values compared to the PDI values.

5.5 Work diagram

When investigating the work diagrams, a more ductile behavior is apparent in the ASR affected cylinders. A less ductile behavior is apparent in the cylinders drilled in restrained direction compared to the unrestrained direction of the ASR affected concrete. This further strengthen the assumption that concrete deteriorate less when exposed to a small constant stress. By comparing the work diagram to the stress/strain relation parallel and perpendicular to cracks reported by Barbosa et al. [19]. It suggests that some alignment of cracks might be present, however to a small degree. Barbosa et al. [19] reported large differences in ductility parallel and perpendicular to cracks. The cylinders drilled from restrained direction showed somewhat less ductile behavior compared to the unrestrained direction. In addition to the less ductile behavior, low NLI values were calculated in cylinders drilled in restrained direction as seen in figure 16, looking at the RP60-Z datapoints. NLI is said to be able to account for the alignment of cracks. This further suggests some alignment of the micro cracks.

5.6 Predicting expansion and mechanical properties

The resulting plots from the SDT show a strong correlation between the indices and expansion, thus pointing to SDT as a good tool to predict expansion level. The calculated SDI, PDI and NLI fit well in with Sanchez result. However, when investigating the relationship between the indices and expansion up to 0.2%, the linear relationship between NLI and expansion disappears. This is problematic, as most real structure are expected to have lower levels of expansions compared to laboratory samples due to the reinforcement and other restraints, which have been shown to reduce the expansion by us and others [7–9]. This points to NLI as a more unreliable parameter when investigating real concrete structures. On the other hand, SDI and PDI shows a strong linear correlation to expansion at low levels of expansion. The effect on the correlation between SDI/PDI/NLI and expansion with expansion levels between 0% to 0.2% can be seen in figure 20A-C, respectively. This disparity between the specter of expansion as a whole and the lower level of expansion by itself suggests that the relation between SDI/PDI and expansion might best be divided into two different phases: first phase presenting a linear dependency up to about 0.2% expansion and second phase from 0.2% expansion and beyond presenting a logarithmic dependency.

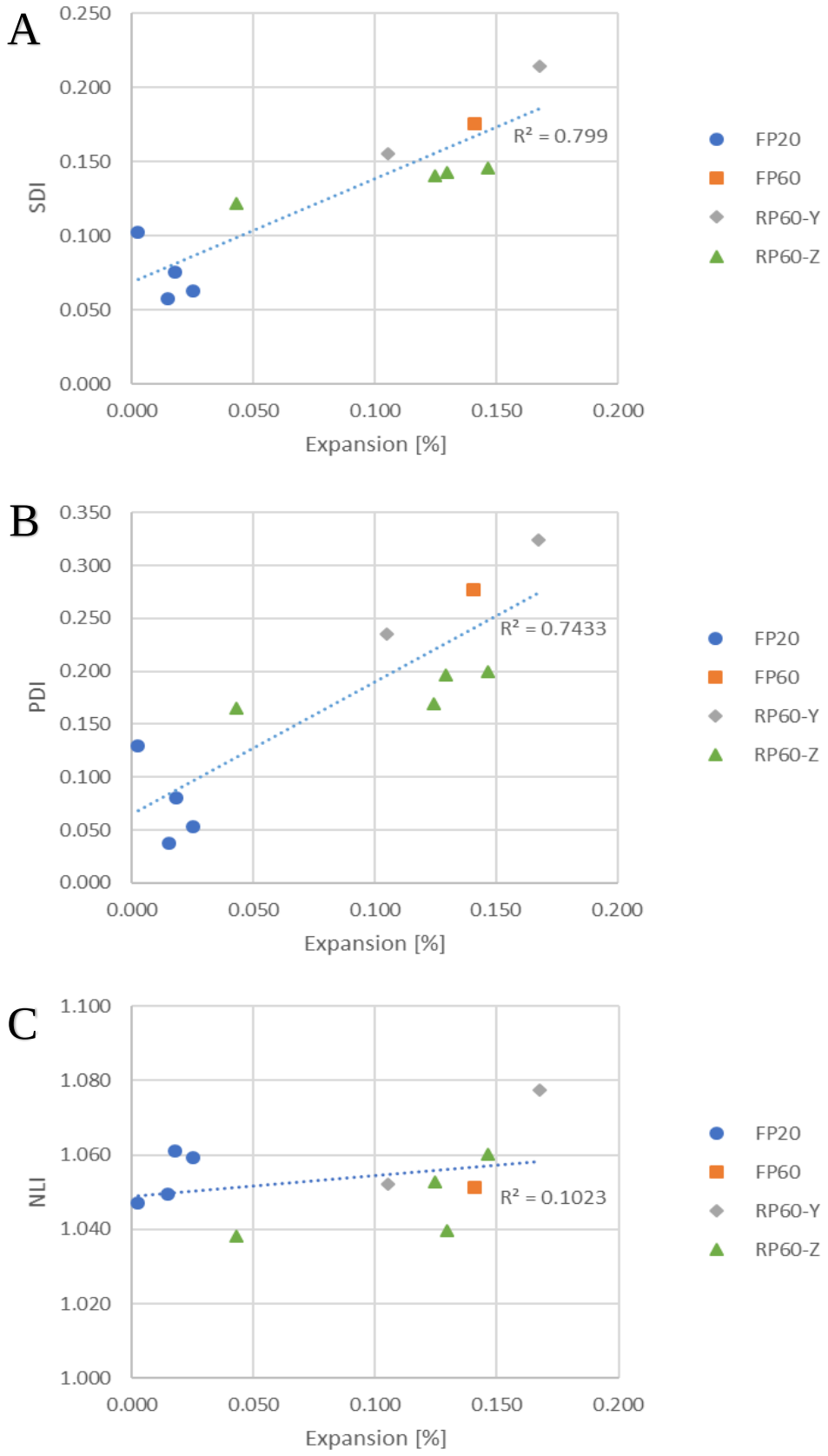

Figure 21. A-C: SDI/PDI/NLI plotted against expansion from 0-0.2% with a linear trend line, respectively.

One major drawback appears when testing previously untested concrete. A calculated SDI value of 0.2 could mean an expansion between 0.025% and 0.2% according to the spread in Sanchez et al. [21] result, illustrated by the area between the yellow dotted lines in figure 19A. In a real structure this could mean an expansion level from almost no expansion to significant expansion. A part of this problem is countered by investigating samples from presumed undamaged part and different expansion level. A logarithmic or linear line, describing the relation to expansion, based on previous work like ours and Sanchez et al. [27], with starting point at the measured value in the presumed undamaged samples could then be used to estimate the expansion in the other samples. More research within the lower level of expansion is needed in order to conclude whether a linear or logarithmic relation should be used.

For SDT to be useful in prediction of expansion and change in concrete properties a clear guideline must be presented. A simple misunderstanding on how to calculate the SDI resulted in about 4 times higher values. The alternative SDI might be a better way to calculate the SDI, as the slop at low expansion level are higher. This means that a small change in calculated index value would not affect the predicted expansion as much. However, there seems to be a bigger spread in the values calculated, while still fitting well with the logarithmic trend line. This would result in a relative larger range of calculated values, and the same problem would arise, that an SDI_{alt} value of e.g. 0.7 could mean expansion between 0.025% and 0.2%. The lack of data regarding SDI_{alt} makes it hard to discuss any further at this point.

6 Remarks to the experimental setup

If similar experiments should be carried out again, the following proposed improvements should be considered.

A more convenient way to adjust the pressure needs to be designed. In our setup the whole equipment had to be taken out of the plastic bucket, before tightening the nuts on the 4 threaded steel bars and then lifted back. The illustration of the setup shows a M32tap bolt through the top steel plate. However, the plate was delivered without the threaded hole ordered, so we proceeded without the tap bolt. The tightening itself is manageable, but the whole setup with concrete sample weighs about 100kg, making the process heavy and tedious work.

Because of the weight of the setup, one should be 4 persons when lifting it according to the Norwegian work directives. However, only 2 persons can lift at the same time due to space limitations. Thus, a lifting tool should be installed, e.g. welding a hook at the top plate. A lifting crane can then be used to lift it in and out of the buckets. In addition, adding the M32 tap bolt would make it unnecessary to lift the setup from the bucket until scheduled testing.

During the experiment 3 measuring knots fell of making expansion measurement impossible. This could for example be prevented by casting them in place or drilling holes where they are glued, giving the glue bigger surface connection to the knots. Another option is to use a more automated measuring system casted inside the concrete samples. The latter would be preferable as it could measure expansion continuously and the treaded steel bars would not be an issue when the measurement are done, however this option is expensive.

The prims standing in the creep machine should be sealed or wrapped in plastic to hinder shrinkage and keeping the moisture level close to 100% RH, hence as equal storage conditions to the samples placed in the reactor as possible. One of the reasons for placing the reference prisms in restraints was to get an estimate on the creep effect from the stress level used. The different storage temperature and humidity made this more of a guess work, especially since humidity highly affects the specific creep level in a sample.

The reactor could be improved by adding an extra fan, which would help circulate the air better. It took some time for the temperature to stabilize inside the reactor after it was opened. A couple of degree warmer close to the air heater was measured before it was stabilized. This resulted in a small difference inside the bucket nearest the air heater and furthest apart. This

difference could be minimized by using 2 buckets less and leaving some space right in front of the air heater empty and added air circulation.

7 Conclusion

Restraints clearly affect the development of ASR in terms of expansion, mechanical properties and degree of damage. The main conclusions are:

- Expansion are hindered in restrained direction, however no transfer of expansion to unrestrained direction is apparent.
- Compressive strength testing shows no clear results. A small reduction of compressive strength in the free prisms exposed to ASR compared to the reference prisms is present. However, the restraints seem to obscure the already small effect, rendering the change and effects on compressive strength hard to predict.
- The reduction of elastic modulus shows a strong correlation with increasing level of expansion. This means that restraints, which prevent some expansion, also prevent some of the reduction of elastic modulus due to ASR.
- The calculated damage indices show a clear reduction of damage in restrained direction, which correspond well with the lower reduction in elastic modulus in restrained direction.
- The ASR affected samples that are free to expand show a more ductile behavior, while the restrained sample show similar behavior as the reference samples in the restrained direction, meaning less ductile behavior. The ductility of the restrained ASR affected samples in the direction perpendicular to the restraint, is similar to the ASR affected samples with free expansion. Both statements are supporting the statement that a restraint (compressive stress) result in less degree of damage.
- Our results strengthen Sanchez et al. [27] proposal that SDT and the calculated indices, SDI and PDI, is a promising tool to assess the degree of damage and predict the expansion in concrete structures. The NLI was unreliable with low level of expansion, rendering it less promising. In addition to the indices, elastic modulus is also an interesting output parameter from the SDT due to the strong correlation with expansion and the more ductile behavior of ASR affected concrete.

To summarize, all output parameters points to a lower degree of damage in restrained direction, except compressive strength which gave unclear results. No increased expansion and damage are found in unrestrained direction. This means that an overall lower impact from

ASR is reported in the restrained prisms compared to the free primes exposed to the same conditions.

In order to make SDT a reliable tool to assess degree of damage in ASR affected concrete structures, more testing needs to be conducted both with and without restraints on different concrete recipes. A more thorough description should also be made on how to run the SDT and how to calculate the different indices. There were some uncertainties regarding how long the maximum and minimum load should be held during the load cycles, and how the indices should be calculated.

References

[1] E.M. Gartner, J.F. Young, D.A. Damidot, I. Jawed, Hydration of Portland cement, Structure and performance of cements 2 (2002) 57–108.

[2] J. Lindgård, Alkali-silica reaction (ASR): Performance testing. Avhandling (ph.d.) - Norges teknisk-naturvitenskapelige universitet, Trondheim, 2013, Norwegian University of Science and Technology Faculty of Natural Sciences and Technology Department of Materials Science and Engineering, Trondheim, 2013.

[3] Statens Vegvesen, Alkalireaksjoner – Karbonfiberforsøk Elgeseter bru: SVV Rapport nr 339, available at https://www.vegvesen.no/_attachment/788811/binary/1015299?fast_title=Nr+339+Alkalireaksjoner+-+Karbonfiberfors%C3%B8k+Elgeseter+bru.pdf (accessed on August 31, 2018).

[4] Statens Vegvesen, Bedre Bruvedlikehold, available at https://www.vegvesen.no/en/professional/research+and+development/better-bridge-maintenance/projects (accessed on December 15, 2017).

[5] D. Stark, Chapter 34: Alkali-Silica Reactions in Concrete, in: J.F. Lamond, J.H. Pielert (Eds.), Significance of tests and properties of concrete & concrete-making materials, ASTM, Philadelphia, PA, 2006, 401-401-9.

[6] M.M. Karthik, J.B. Mander, S. Hurlebaus, ASR/DEF related expansion in structural concrete: Model development and validation, Construction and Building Materials 128 (2016) 238–247.

[7] M. Berra, G. Faggiani, T. Mangialardi, A.E. Paolini, Influence of stress restraint on the expansive behaviour of concrete affected by alkali-silica reaction, Cement and Concrete Research 40 (9) (2010) 1403–1409.

[8] B.P. Gautam, D.K. Panesar, A new method of applying long-term multiaxial stresses in concrete specimens undergoing ASR, and their triaxial expansions, Mater Struct 49 (9) (2016) 3495–3508.

[9] A.E.K. Jones, L.A. Clark, The effects of restraint on ASR expansion of reinforced concrete, Magazine of Concrete Research 48 (174) (1996) 1–13.

[10] A.E.K. Jones, L.A. Clark, The effects of ASR on the properties of concrete and the implications for assessment, Engineering Structures 20 (9) (1998) 785–791.

[11] P. Rivard, M.-A. Bérubé, J.-P. Ollivier, G. Ballivy, Alkali mass balance during the accelerated concrete prism test for alkali–aggregate reactivity, Cement and Concrete Research 33 (8) (2003) 1147–1153.

[12] P. Rivard, M.A. Bérubé, J.P. Ollivier, G. Ballivy, Decrease of pore solution alkalinity in concrete tested for alkali-silica reaction, Mater Struct 40 (9) (2007) 909–921.

[13] J. Lindgård, M.D.A. Thomas, E.J. Sellevold, B. Pedersen, Ö. Andiç-Çakır, H. Justnes, T.F. Rønning, Alkali–silica reaction (ASR)—performance testing: Influence of specimen pre-treatment, exposure conditions and prism size on alkali leaching and prism expansion, Cement and Concrete Research 53 (2013) 68–90.

[14] R.V. Balendran, W.H. Martin-Buades, The influence of high temperature curing on the compressive, tensile and flexural strength of pulverized fuel ash concrete, Building and Environment 35 (5) (2000) 415–423.

[15] K. Tan, O.E. Gjorv, Performance of concrete under different curing conditions, Cement and Concrete Research 26 (3) (1996) 355–361.

[16] S.N. Shoukry, G.W. William, B. Downie, M.Y. Riad, Effect of moisture and temperature on the mechanical properties of concrete, Construction and Building Materials 25 (2) (2011) 688–696.

[17] J.J. Brooks, 30-year creep and shrinkage of concrete, Magazine of Concrete Research 57 (9) (2005) 545–556.

[18] L.F.M. Sanchez, B. Fournier, M. Jolin, J. Bastien, Evaluation of the stiffness damage test (SDT) as a tool for assessing damage in concrete due to ASR: Test loading and output responses for concretes incorporating fine or coarse reactive aggregates, Cement and Concrete Research 56 (2014) 213–229.

[19] R.A. Barbosa, S.G. Hansen, K.K. Hansen, L.C. Hoang, B. Grelk, Influence of alkali-silica reaction and crack orientation on the uniaxial compressive strength of concrete cores from slab bridges, Construction and Building Materials 176 (2018) 440–451.

[20] H. Marzouk, S. Langdon, The effect of alkali-aggregate reactivity on the mechanical properties of high and normal strength concrete, Cement and Concrete Composites 25 (4-5) (2003) 549–556.

[21] G. Giaccio, R. Zerbino, J.M. Ponce, O.R. Batic, Mechanical behavior of concretes damaged by alkali-silica reaction, Cement and Concrete Research 38 (7) (2008) 993–1004.

[22] Hans Stemland, Marit Haugen, Laboratorieundersøkelser av utborede betongkjerner. fra Fiborg, Holsand og Hotran bru samt Holte viadukt, SINTEF, 2017.

[23] Prøving av herdnet betong: Testing hardened concrete determination of secant modulus of elasticity in compression, Standard Norge, Lysaker, 2013.

[24] T.M. Chrisp, P. Waldron, J.G.M. Wood, Development of a non-destructive test to quantify damage in deteriorated concrete, Magazine of Concrete Research 45 (165) (1993) 247–256.

[25] C09 Committee, Test Method for Static Modulus of Elasticity and Poissons Ratio of Concrete in Compression, ASTM International, West Conshohocken, PA.

[26] L.F.M. Sanchez, B. Fournier, M. Jolin, J. Bastien, D. Mitchell, Practical use of the Stiffness Damage Test (SDT) for assessing damage in concrete infrastructure affected by alkali-silica reaction, Construction and Building Materials 125 (2016) 1178–1188.

[27] L.F.M. Sanchez, B. Fournier, M. Jolin, D. Mitchell, J. Bastien, Overall assessment of Alkali-Aggregate Reaction (AAR) in concretes presenting different strengths and incorporating a wide range of reactive aggregate types and natures, Cement and Concrete Research 93 (2017) 17–31.

[28] E.R. Giannini, L.F.M. Sanchez, A. Tuinukuafe, K.J. Folliard, Characterization of concrete affected by delayed ettringite formation using the stiffness damage test, Construction and Building Materials 162 (2018) 253–264.

[29] Statens Vegvesen, Alkalireaksjoner - Feltforsøk med overflatebehandling: SVV Rapport nr 465, available at https://www.vegvesen.no/_attachment/1134224/binary/1081861?fast_title=Nr+465+Alkalireaksjoner+-+Feltfors%C3%B8k+med+overflatebehandling.pdf (accessed on December 15, 2017).

[30] P.J. Nixon, I. Sims, RILEM Recommendations for the Prevention of Damage by Alkali-Aggregate Reactions in New Concrete Structures, Springer Netherlands, Dordrecht, 2016.

[31] H. Kagimoto, Y. Yasuda, M. Kawamura, ASR expansion, expansive pressure and cracking in concrete prisms under various degrees of restraint, Cement and Concrete Research 59 (2014) 1–15.

[32] Prøving av herdnet betong, 1st ed., Standard Norge, Oslo, 2009.

[33] Eurokode 2: Prosjektering av betongkonstruksjoner: Eurocode 2: Design of concrete structures. Part 1-1: General rules and rules for buildings, Standard Norge, Lysaker, 2008.

[34] Z.P. Bazant, S.S. Kim, NONLINEAR CREEP OF CONCRETE - ADAPTATION AND FLOW, ASCE J Eng Mech Div 105 (3) (1979) 429–446.

[35] R. N. Swamy and M. M. Al-Asali, Engineering Properties of Concrete Affected by Alkali-Silica Reaction, Materials Journal 85 (5).

[36] T. Ahmed, E. Burley, S. Rigden, A.I. Abu-Tair, The effect of alkali reactivity on the mechanical properties of concrete, Construction and Building Materials 17 (2) (2003) 123–144.

Appendix A

150 l I + II

SINTEF | **Prøveblanding i betong** | side 1 | Prosjektnr. 102017920-1

Oppdrag fra NTNU | Journalnr.

Blanding nr. | Konsistens | Vekt reg.nr:

Delmaterialer	Deler	Tørr vekt, kg	Fukt, %	Innveid vekt, kg	Vann, kg
Sement INNOSTRI	A-4/334	68,550	—	✓ 68,550	—
Årdal 0/4		100,050	(3.1) 3,0	✓ 103,152	3,002
— " — 4/8		25,800	(1.2) 0,7	✓ 26,110	0,181
— " — 8/11		77,700	(0.6) 0,3	✓ 78,166	0,233
— " — 11/16		51,750	(0.5) 0,1	✓ 52,009	0,052

Vekt reg.nr:

Tilsetningsstoff	Deler	Konsentrert, kg	10 % oppløsning, kg	Vann, kg
SIKA FB-2	A-405-2	0,235		
			Tilsatt blandevann, kg	29.082

Totalt vanninnhold, oppgitt av saksbehandler (eks vann i konsentrerte tilsetningsstoffer): 32.530

Utstøpte prøvestykker, antall og dimensjoner. Utstøpt kl: 6/3 -18

..... stk .....cm .....merket .....prøves .....ved alder .....døgn
..... stk .....cm .....merket .....prøves .....ved alder .....døgn
..... stk .....cm .....merket .....prøves .....ved alder .....døgn
..... stk .....cm .....merket .....prøves .....ved alder .....døgn

v/c	v/c + s	Synkmål	Utbredelsesmål	Luftinnhold		Romdensitet	
		175 mm		2,8%	2,9%	2390	2375

Betongblanding og målinger utført av: KL / EF

Delmaterialer i kg/m³ betong

Vekt reg.nr:	Sement	Silika	Vann						

Nr	Vekt i g ved avform	Vekt i g ved prøving	Lastinnstilling/maskin Operatør/Dato	Bruddlast (kN eller kp)	Trykkfasthet MPa	Middel MPa	Største n. steinstr	Brudd-form*	Alder døgn

* Se NS-EN 12390-3 for koding av bruddform.

Rev. 2014-01-20 GK

891 Prøveblanding i betong

Appendix B

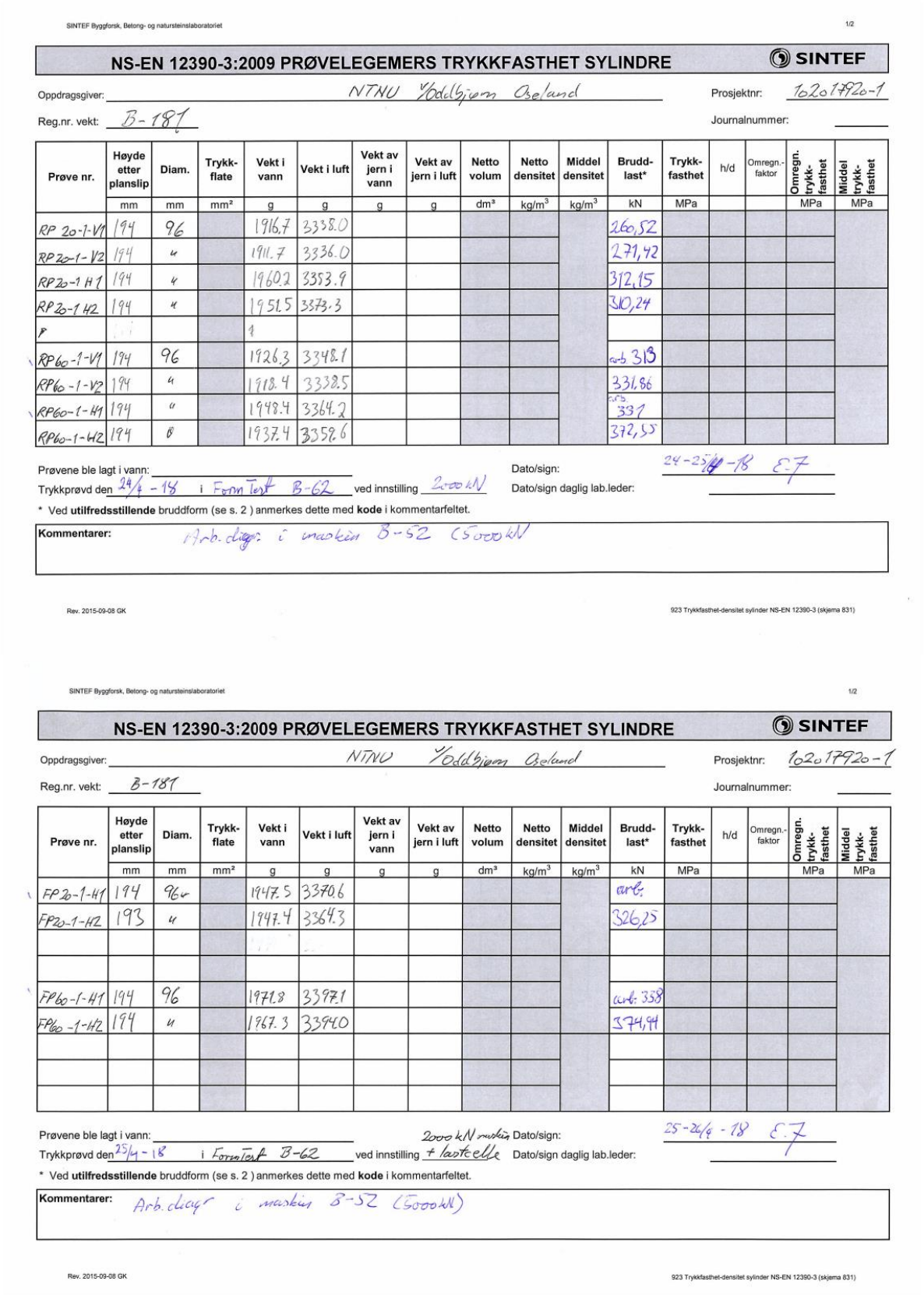

SINTEF Byggforsk, Betong- og natursteinslaboratoriet 1/2

NS-EN 12390-3:2009 PRØVELEGEMERS TRYKKFASTHET SYLINDRE SINTEF

Oppdragsgiver: NTNU v/Oddbjørn Øsetund Prosjektnr: 102017920-1

Reg.nr. vekt: B-181 Journalnummer:

Prøve nr.	Høyde etter planslip	Diam.	Trykk-flate	Vekt i vann	Vekt i luft	Vekt av jern i vann	Vekt av jern i luft	Netto volum	Netto densitet	Middel densitet	Brudd-last*	Trykk-fasthet	h/d	Omregn.-faktor	Omregn. trykk-fasthet	Middel trykk-fasthet
	mm	mm	mm²	g	g	g	g	dm³	kg/m³	kg/m³	kN	MPa			MPa	MPa
RP 20-1-V1	194	96		1916.7	3338.0						260,52					
RP 20-1-V2	194	"		1911.7	3336.0						271,42					
RP 20-1 H1	194	"		1960.2	3353.9						312,15					
RP 20-1 H2	194	"		1951.5	3373.3						310,24					
F																
RP 60-1-V1	194	96		1926.3	3348.1						anb 313					
RP 60-1-V2	194	"		1918.4	3338.5						331,86					
RP 60-1-H1	194	"		1948.4	3364.2						anb 337					
RP 60-1-H2	194	"		1937.4	3359.6						372,55					

Prøvene ble lagt i vann: Dato/sign: 24-25/4-18 E.T

Trykkprøvd den 24/4-18 i Form Test B-62 ved innstilling 2000 kN Dato/sign daglig lab.leder:

* Ved **utilfredsstillende** bruddform (se s. 2) anmerkes dette med **kode** i kommentarfeltet.

Kommentarer: Arb. dager i maskin B-52 (5000 kN

Rev. 2015-09-08 GK 923 Trykkfasthet-densitet sylinder NS-EN 12390-3 (skjema 831)

SINTEF Byggforsk, Betong- og natursteinslaboratoriet 1/2

NS-EN 12390-3:2009 PRØVELEGEMERS TRYKKFASTHET SYLINDRE SINTEF

Oppdragsgiver: NTNU v/Oddbjørn Øsetund Prosjektnr: 102017920-1

Reg.nr. vekt: B-181 Journalnummer:

Prøve nr.	Høyde etter planslip	Diam.	Trykk-flate	Vekt i vann	Vekt i luft	Vekt av jern i vann	Vekt av jern i luft	Netto volum	Netto densitet	Middel densitet	Brudd-last*	Trykk-fasthet	h/d	Omregn.-faktor	Omregn. trykk-fasthet	Middel trykk-fasthet
	mm	mm	mm²	g	g	g	g	dm³	kg/m³	kg/m³	kN	MPa			MPa	MPa
FP 20-1-H1	194	96		1947.5	3370.6						arb.					
FP 20-1-H2	193	"		1947.4	3364.3						326,25					
FP 60-1-H1	194	96		1971.8	3397.1						arb: 338					
FP 60-1-H2	194	"		1967.3	3394.0						374,94					

Prøvene ble lagt i vann: 2000 kN maskin Dato/sign: 25-26/4-18 E.T

Trykkprøvd den 25/4-18 i Form Test B-62 ved innstilling + lastcelle Dato/sign daglig lab.leder:

* Ved **utilfredsstillende** bruddform (se s. 2) anmerkes dette med **kode** i kommentarfeltet.

Kommentarer: Arb. dager i maskin B-52 (5000 kN)

Rev. 2015-09-08 GK 923 Trykkfasthet-densitet sylinder NS-EN 12390-3 (skjema 831)

SINTEF Byggforsk, Betong- og natursteinslaboratoriet 1/2

NS-EN 12390-3:2009 PRØVELEGEMERS TRYKKFASTHET SYLINDRE

SINTEF

Oppdragsgiver: _____ Prosjektnr: _____

Reg.nr. vekt: B-181 Journalnummer: _____

Prøve nr.	Høyde etter planslip	Diam.	Trykk-flate	Vekt i vann	Vekt i luft	Vekt av jern i vann	Vekt av jern i luft	Netto volum	Netto densitet	Middel densitet	Brudd-last*	Trykk-fasthet	h/d	Omregn.-faktor	Omregn. trykk-fasthet	Middel trykk-fasthet
	mm	mm	mm²	g	g	g	g	dm³	kg/m³	kg/m³	kN	MPa			MPa	MPa
RP60-2-21	193	96		1902,9	3317,6						ARB.*					
RP60-2-22	193	97		1913,6	3325,3						324.7*				44.8	
RP60-2-Y1	193	97		1922,8	3334.3						ARB.*					
RP60-2-Y2	193	96		1911.4	3326,6						360.7				49.8	
RP20-2-21	193	96		1897,7	330816						276,3				38.2	
RP20-2-22	193	97		1907,4	3318,9						277				38	
RP20-2-Y1	192	97		1919,3	3323,8						328				45	
RP20-2-Y2	192	97		1915,9	3321,8						330				46	

Prøvene ble lagt i vann: _____ Dato/sign: _____

Trykkprøvd den _____ i B-62 ved innstilling 2000 kN Dato/sign daglig lab.leder: _____

* Ved **utilfredsstillende** bruddform (se s. 2) anmerkes dette med **kode** i kommentarfeltet.

Kommentarer:

Rev. 2015-09-08 GK 923 Trykkfasthet-densitet sylinder NS-EN 12390-3 (skjema 831)

SINTEF Byggforsk, Betong- og natursteinslaboratoriet 1/2

NS-EN 12390-3:2009 PRØVELEGEMERS TRYKKFASTHET SYLINDRE

SINTEF

Oppdragsgiver: _____ Prosjektnr: _____

Reg.nr. vekt: B-181 Journalnummer: _____

Prøve nr.	Høyde etter planslip	Diam.	Trykk-flate	Vekt i vann	Vekt i luft	Vekt av jern i vann	Vekt av jern i luft	Netto volum	Netto densitet	Middel densitet	Brudd-last*	Trykk-fasthet	h/d	Omregn.-faktor	Omregn. trykk-fasthet	Middel trykk-fasthet
	mm	mm	mm²	g	g	g	g	dm³	kg/m³	kg/m³	kN	MPa			MPa	MPa
FP60-2-21	192	96		1913,0	3317,4						ARB.*					
FP60-2-22	192	96		1911,8	3316,5											
		906														
FP20-2-21	193	96		1926,2	3335,8						ARB.*					
FP20-2-22	193	96		1919,3	3329,2						463*				461	

Prøvene ble lagt i vann: _____ Dato/sign: _____

Trykkprøvd den 29.05.18 i B-62 ved innstilling 2000 kN Dato/sign daglig lab.leder: _____

* Ved **utilfredsstillende** bruddform (se s. 2) anmerkes dette med **kode** i kommentarfeltet.

Kommentarer:

Rev. 2015-09-08 GK 923 Trykkfasthet-densitet sylinder NS-EN 12390-3 (skjema 831)

SINTEF Byggforsk, Betong- og natursteinslaboratoriet 1/2

NS-EN 12390-3:2009 PRØVELEGEMERS TRYKKFASTHET SYLINDRE — SINTEF

Oppdragsgiver: Prosjektnr:

Reg.nr. vekt: Journalnummer:

Prøve nr.	Høyde etter planslip	Diam.	Trykk-flate	Vekt i vann	Vekt i luft	Vekt av jern i vann	Vekt av jern i luft	Netto volum	Netto densitet	Middel densitet	Brudd-last*	Trykk-fasthet	h/d	Omregn.-faktor	Omregn. trykk-fasthet	Middel trykk-fasthet
	mm	mm	mm²	g	g	g	g	dm³	kg/m³	kg/m³	kN	MPa			MPa	MPa
[illegible]											351.6					
FP20-3-Z1	189.5	94.8		1848.5	3178						351.6	49.8				
FP20-3-Z2	189.5	94.8		1853.8	3183.2						334.6	47.4				
* RP20-3-Y1	190.4	94.8		1846.6	3181.1						arb.	arb.				
Y2	190.5	94.8		1852.4	3187.7						313	44.3				
RP20-3-Z1	191.6	94.8		1846.6	3188.4						arb.	arb.				
o Z2	191.5	94.8		1845.9	3186.5						302.9	42.9				

Prøvene ble lagt i vann: Dato/sign:

Trykkprøvd den i ved innstilling Dato/sign daglig lab.leder:

* Ved **utilfredsstillende** bruddform (se s. 2) anmerkes dette med **kode** i kommentarfeltet.

Kommentarer:

Rev. 2015-09-08 GK

* Glemte å nulle ut giver
o Kun 4 sykler

923 Trykkfasthet-densitet sylinder NS-EN 12390-3 (skjema 831)

SINTEF Byggforsk, Betong- og natursteinslaboratoriet 1/2

NS-EN 12390-3:2009 PRØVELEGEMERS TRYKKFASTHET SYLINDRE — SINTEF

Oppdragsgiver: Prosjektnr:

Reg.nr. vekt: Journalnummer:

Prøve nr.	Høyde etter planslip	Diam.	Trykk-flate	Vekt i vann	Vekt i luft	Vekt av jern i vann	Vekt av jern i luft	Netto volum	Netto densitet	Middel densitet	Brudd-last*	Trykk-fasthet	h/d	Omregn.-faktor	Omregn. trykk-fasthet	Middel trykk-fasthet
	mm	mm	mm²	g	g	g	g	dm³	kg/m³	kg/m³	kN	MPa			MPa	MPa
RP60-4-Y1	190.3	94.8		1848.4	3185						arb.	arb.				
Y2	190.4	94.8		1851.9	3189.1						339.4	48.1				
Z1	190.5	94.8		1837.9	3175.2						arb.	arb.				
Z2	190.6	94.8		1828.0	3165.6						328.8	46.6				
					[illegible]						311.1					
FP60-4-Z1	189.7	94.8		1859.2	3190						311.1	44.1				
Z2	189.4	94.8		1851.3	3182.3						323.5	45.8				

Prøvene ble lagt i vann: Dato/sign:

Trykkprøvd den i ved innstilling Dato/sign daglig lab.leder:

* Ved **utilfredsstillende** bruddform (se s. 2) anmerkes dette med **kode** i kommentarfeltet.

Kommentarer:

Rev. 2015-09-08 GK

923 Trykkfasthet-densitet sylinder NS-EN 12390-3 (skjema 831)

SINTEF Byggforsk, Betong- og natursteinslaboratoriet 1/2

NS-EN 12390-3:2009 PRØVELEGEMERS TRYKKFASTHET SYLINDRE

SINTEF

Oppdragsgiver: NTNU v/Oddbjørn Øseland Prosjektnr:

Reg.nr. vekt: B-181 Journalnummer:

Prøve nr.	Høyde etter planslip	Diam.	Trykk-flate	Vekt i vann	Vekt i luft	Vekt av jern i vann	Vekt av jern i luft	Netto volum	Netto densitet	Middel densitet	Brudd-last*	Trykk-fasthet	h/d	Omregn.-faktor	Omregn. trykk-fasthet	Middel trykk-fasthet
	mm	mm	mm²	g	g	g	g	dm³	kg/m³	kg/m³	kN	MPa			MPa	MPa
RP20-4-Z1	94	190		1872,0	8223,1						527					
-11--Z2	95	190		1863,4	3212,3						51,4					
-11--Z3	95	190		1856,1	3207,4						47,5					
-11--Z4	95	190		1862,8	3212,8						46,6					
RP60-3-Z1	95	190		1843,9	3155,6						42,1					
-11--Z2	95	190		1850,5	3201,2						43,1					
-11--Z3	95	190		1830,1	3181,7						39,1					
-11--Z4	94	190		1827,3	3180,5						40,1					

Prøvene ble lagt i vann: Dato/sign:

Trykkprøvd den i FORMTEST B-62 ved innstilling 200kN Dato/sign daglig lab.leder:

* Ved **utilfredsstillende** bruddform (se s. 2) anmerkes dette med **kode** i kommentarfeltet.

Kommentarer: ARB. diagr. i B-52 (5000kN

Rev. 2015-09-08 GK 923 Trykkfasthet-densitet sylinder NS-EN 12390-3 (skjema 831)

SINTEF Byggforsk, Betong- og natursteinslaboratoriet 1/2

NS-EN 12390-3:2009 PRØVELEGEMERS TRYKKFASTHET SYLINDRE

SINTEF

Oppdragsgiver: NTNU v/Oddbjørn Øseland Prosjektnr:

Reg.nr. vekt: B-181 Journalnummer:

Prøve nr.	Høyde etter planslip	Diam.	Trykk-flate	Vekt i vann	Vekt i luft	Vekt av jern i vann	Vekt av jern i luft	Netto volum	Netto densitet	Middel densitet	Brudd-last*	Trykk-fasthet	h/d	Omregn.-faktor	Omregn. trykk-fasthet	Middel trykk-fasthet
	mm	mm	mm²	g	g	g	g	dm³	kg/m³	kg/m³	kN	MPa			MPa	MPa
RP20-4-Z1	190	95		1822,8	3173,0						ARB					
-11--Z2	190	95		1813,6	3162,4						304,1	42,9				
RP20-4-Y1	190	95		1804,2	3157,6						ARB					
-11--Y2	190	95		1808,5	3159,2						314,7	44,4				
RP60-3-Z1	190	95		1826,5	3176,8						ARB					
-11--Z2	190	95		1830,0	3181,8						318,4	45,9				
RP60-3-Y1	190	95		1827,2	3178,5						ARB					
-11-Y2	190	95		1833,9	3184,5						325,5	46,9				

Prøvene ble lagt i vann: Dato/sign:

Trykkprøvd den i FORMTEST B62 ved innstilling 200kN Dato/sign daglig lab.leder:

* Ved **utilfredsstillende** bruddform (se s. 2) anmerkes dette med **kode** i kommentarfeltet.

Kommentarer: ARB. DIAGR. B-52

Rev. 2015-09-08 GK 923 Trykkfasthet-densitet sylinder NS-EN 12390-3 (skjema 831)

Appendix C

Sample	Days [d]	expan-sion [%]	fc [MPa]	E_c [MPa]	SDI	PDI	NLI	SDI_{alt}
FP20	52	0.003	42.7	32045	0.102	0.129	1.047	0.437
	83	0.018	46.7	34081	0.076	0.081	1.061	0.324
	118	0.025	46.8	33715	0.063	0.053	1.059	0.268
	160	0.015	50.7	34340	0.057	0.037	1.050	0.243
FP60	52	0.141	50.0	24745	0.176	0.277	1.051	0.730
	83	0.285	46.7	19465	0.223	0.299	1.118	0.874
	118	0.346	44.0	17996	0.218	0.291	1.171	0.879
	160	0.469	41.7	16477	0.234	0.325	1.201	0.940
RP60-Y	52	0.105	49.4	27629	0.155	0.235	1.052	0.653
	83	0.168	50.4	22069	0.215	0.324	1.077	0.869
	118	0.327	46.4	20027	0.217	0.301	1.142	0.867
	160	0.353	45.6	18476	0.217	0.281	1.135	0.858
RP60-Z	52	0.043	45.2	28059	0.122	0.165	1.038	0.517
	83	0.130	45.6	25576	0.140	0.197	1.040	0.599
	118	0.147	44.8	24543	0.146	0.200	1.060	0.608
	160	0.125	44.6	24079	0.141	0.169	1.053	0.589
RP20-Y	52	-0.031	43.0	33414	0.076	0.099	1.075	0.373
	83	-0.044	46.1	34514	0.068	0.097	1.058	0.334
	118	-0.042	42.9	33405	0.070	0.096	1.058	0.343
	160	-0.053	43.3	32294	0.070	0.110	1.057	0.345
RP20-Z	52	-0.059	36.7	31788	0.090	0.117	1.097	0.442
	83	-0.068	38.8	32512	0.081	0.109	1.067	0.401
	118	-0.072	41.2	32877	0.069	0.087	1.062	0.330
	160	-0.077	42.1	32820	0.064	0.083	1.053	0.315